1.1. Introduction

The multifaceted perovskite oxides with general formula ABO_3 (where A can be mono, di, tri and B can be di, tri, tetra, or penta-valent cations) are special class of materials which can exhibit a range of extensively diverse physical and chemical properties such as ferroelectricity, piezoelectricity, electrocatalytic, electro-optic, ferromagnetism, antiferromagnetism, magnetocaloric, metallic, semiconducting and insulating, etc. The most beautiful feature of the perovskite structure (ABO_3,) is that it can accommodate variety of cations at A and B-sites having different ionic sizes and valencies, leading to a variety of physical properties. Due to the extensive range of physical properties, the multifunctional perovskite oxides, offer innumerable applications for example ferroelectric and magnetic memories, piezoelectric transducers and actuators, colossal magnetoresistance, materials for optical fibers and electro-optic devices, positive temperature coefficient of resistance, hybrid solar and solid oxide fuel cells, display devices and phosphors, sensors etc. [Uchino (2000); Eerenstien et al. (2006); Coey et al. (1999); Minh et al. (1993)]. They also display attractive structural and magnetic phase transitions involving incredibly rich chemistry and physics.

The manganese based perovskite oxides having common molecular formula $RMnO_3$ (where R is a trivalent or divalent cation and Mn exists in the trivalent or tetravalent state) are recognized as perovskite manganites. If site R is partially occupied by two different cations, one divalent (A) and another trivalent cation (R), then Mn atom exhibits mixed ionization states, i.e., Mn^{3+} and Mn^{4+} in compounds. The perovskite manganites having mixed valence state of Mn-atom are known as mixed-valence perovskite manganites. The rare earth based mixed-valence perovskite manganites $R_{1-x}A_xMnO_3$ (R = La, Pr, Nd, Sm, Eu, Gd, etc. and A = Ca, Sr, Ba, etc.), are investigated extensively due to their interesting crystal structure and magnetic phase

transition behaviors as a function of composition, temperature, magnetic field, electric field, strain, pressure etc. Many mixed valence perovskite manganites exhibit orbital and charge ordering which may be coupled to each other, leading to multifaceted physical properties [Tokura (2000); Tokura et al. (2000); Dagotto et al. (2001); Dagotto (2003); Murakami (2003)]. For this Ph.D. thesis, we have investigated Mn-site substituted mixed-valence perovskite manganites which are being studied extensively in recent years.

This chapter presents a brief introduction and concise overview to the mixed-valence perovskite manganites ($R_{1-x}A_xMnO_3$), and Mn-site substituted manganites along with the emphasis on how the physical and magnetic properties progress as a function of composition, particle size, and temperature. This chapter also deals with the consequences of modifications in the crystal structure on controlling electrical transport and magnetic properties of perovskite manganites. The physical properties of various mixed-valence perovskite manganites have been illustrated along with different phenomena exhibited by these compounds. The structural and magnetic phase transitions behavior of some important manganites have been discussed in detail. In addition, the effect of reduction of crystallite size on physical behaviors in nano-structured manganites is also discussed.

1.2. General Description of Perovskite Oxides

Perovskite is an oxide mineral of calcium titanium, having chemical formula $CaTiO_3$. This mineral was discovered in the Ural Mountains of Russia by Gustav Rose in 1839 and is named after Russian mineralogist Lev Perovski. The term “perovskite structure” and “perovskite” are frequently used in a similar sense; but the proper perovskite is formed of calcium (Ca), titanium (Ti) and oxygen (O) in the form of $CaTiO_3$, whereas, a perovskite structure is anything that has general formula of the form

ABX_3 (A = divalent cation, B = tetravalent cation and X = divalent anion) and the crystallographic structure similar as perovskite. The ideal perovskite structure has the cubic crystal structure with $Pm\bar{3}m$ space group (No. 221). The ions in the $Pm\bar{3}m$ space group for the perovskite oxide occupy the Wyckoff positions as "A" in 1(a) sites at (0, 0, 0), "B" in 1(b) sites at (1/2,1/2,1/2) and "O" in 3(c) sites at (0, 1/2,1/2). An equivalent description of the structure can be "A" in 1(a) sites at (1/2, 1/2, 1/2), "B" in 1(b) sites at (0, 0, 0) and "O" in 3(c) sites at (1/2, 0, 0). In the ideal cubic perovskite structure, A and B ions are located at the center of cuboctahedron (dodecahedral site) and octahedron formed by the O ions, i.e., AO_{12} and BO_6, respectively. The schematic diagram/sketch of the cubic perovskite structure is shown in **Fig. 1.1**.

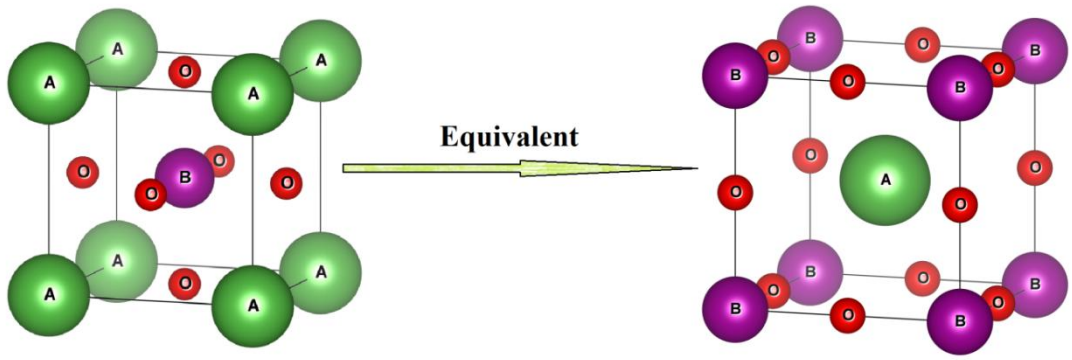

Figure 1.1: Ideal ABO_3 perovskite unit cell representing "A" atoms at (0, 0, 0) or (1/2, 1/2, 1/2), the "B" atoms (1/2, 1/2, 1/2) or (0, 0, 0) and "O" atoms at (0, 1/2, 1/2) or (1/2, 0, 0) positions in cubic lattice.

In 1926, Goldschmidt [Goldschmidt et al. (1926)] defined a new parameter denoted by "t" and now well known as structural tolerance factor or simply tolerance factor, to predict the stability (deformability from the ideal cubic structure) of the perovskite structure. The expression for the estimation of tolerance factor t, associated with the ionic radii, is obtained by using the concept of well known closed packed theory of ions. The tolerance factor is defined as:

$$t = \frac{(r_A + r_O)}{\sqrt{2}(r_B + r_O)} \quad (1.1)$$

where, r_A, r_B and r_O are the ionic radii of A, B and O atoms under appropriate coordination environment, respectively. For a stable perovskite structure, the value of t should lie in the range of $0.88 < t < 1.05$. For $t = 1$, the perovskite structure is anticipated to adopt the ideal cubic symmetry ($Pm\bar{3}m$ space group). For $t > 1$, the B atom is too small for the oxygen octahedron (BO_6) so that the structure will build up a small polar distortion in the structure, as appears in $BaTiO_3$. On the other hand, when $t < 1$, the A atom is small for the oxygen cuboctahedral coordination (AO_{12}) and cannot effectively bond with all twelve adjoining O atoms. If the value of t is only slightly less than one, then the tilting and rotations of the oxygen octahedra (BO_6) will be favored as is the case with $CaTiO_3$ [Yashima et al. (2009)].

1.3. Crystal Structure and Properties of Perovskite Manganites

The mixed-valence perovskite manganese oxides, which are usually identified as manganites, continue to be an essential part of the topic for the research in the field of condensed matter physics and materials science due to their important scientific phenomena as well as promising technological applications [Rao et al. (1998); Dagotto (2002); Tokura (2006)]. Although manganites have an extended history of research which started in the middle of the 20^{th} century with the revolutionary works of Jonker and Van Santen (1950), Van Santen and Jonker (1950), Wollan and Koehler (1955) etc., but it received renewed interest around two decades back after observation of colossal magnetoresistance (CMR), a phenomenon where zero field resistance could be suppressed up to a couple of orders by the application of magnetic field, opening possibilities for important technological applications. Additionally, the phenomenon of CMR has significance similar to the high-temperature (T_C) superconductivity, which has been observed in cuprates another important member of transition metal oxide

(TMO) family. Further, perovskite manganites exhibit rich phase diagrams, exhibiting various phases and phase transitions, with unusual coupling between spin, charge, orbital and lattice degrees of freedom that have further motivated to both experimentalists and theoreticians to improve their understanding related to structural, transport and magnetic properties in the correlated electron systems.

The physical behaviors of mixed-valence manganites are mostly affected by two very important parameters: first band filling (or doping concentration), and the second bandwidth of e_g electrons. These parameters can be controlled up to a significant extent by changing the chemical composition of the manganite, whereas, the band filling parameter is controlled by doping of divalent atoms at R/A-site, and bandwidth of e_g electrons is decided by the different combination of R and A ions, which changes the structure as well as the Mn-O bond lengths and Mn-O-Mn bond angles directly by affecting conduction electron concentration in Mn-O-Mn network. The parent rare earth (trivalent) manganites with x = 0 have only Mn^{3+} ions and exhibit generally antiferromagnetic (AFM) and insulating behavior (I), but with successive doping of holes at R-site, create an equal amount of Mn^{4+} ions in the system, forming mixed-valence manganites. This evolves various electronic and magnetic phases, crystal structures and physical properties. The mixed-valence manganites mostly show ferromagnetic (FM) and metallic property (M). The ferromagnetism observed in these systems beyond a certain concentration of Mn^{4+} ions was initially explained by Zener on the basis of double exchange (DE) phenomenon [Zener (1951)], and later it was further extended by De Gennes (1960) and Anderson and Hasegawa (1955). Although the DE mechanism, which is linked with the ferromagnetism (FM) and metallicity (M) was fairly successful in explaining a variety of properties such as FM, CMR phenomenon, metal-insulator transition in early days, later on various discrepancies

were observed between the theoretical predictions and experimental results for several manganite systems. These discrepancies include an incorrect prediction for temperature variation of resistivity; wrong evaluation of Curie temperature etc. but variety of interesting phenomena like charge ordering (CO), orbital ordering (OO), ferromagnetic insulator, Jahn-Teller distortion, etc. were invoked to explain the observed physical properties in manganites. One more addition to this list is the occurrence of phase separation (PS), where the sub-micrometer sized FM-M and AFM-I phases coexist spontaneously [Dagotto (2002); Moreo et al. (1999)]. Phase separation in perovskite manganites has been studied widely in both theoretical and experimental frontiers in last few years, and experimental confirmation for the same has been provided for the manganites with various compositions [Dagotto (2002)]. Half doped mixed-valence (x = 0.5) compounds are found to be very susceptible to this phase coexistence phenomenon as they offer an equivalent energy scale for coexisting FM and AFM phases. In addition, quenched disorder is found to have important influence on phase separation, as recent simulation work has proposed chemical disorder driven inhomogeneous phase with coexistence of competing phases separated by first-order phase transition in metal oxides such as manganites and cuprates [Burgy et al. (2001)].

In view of the foregoing, for the present thesis work, we have investigated the effects of doping of non-magnetic ion such as Ti^{4+} at Mn-site in $R_{1-x}A_xMnO_3$ ($R = La^{3+}$, $Nd^{3+,}$ and $A = Ba^{2+}$) mixed-valence manganites, on the structural and magnetic phase transitions. The effect of particle size in nanocrystalline form of these systems is also investigated.

1.4. Categorization of Magnetic Materials

The diversity in the magnetic behaviors, displayed by different classes of materials, offers lots of possibilities for experimental as well as the theoretical studies. The

magnetic properties of solids originate due to the motion of the electrons and due to permanent magnetic moments of the atoms and electrons. Magnetic behavior is determined mainly by the electronic structure of the materials which offers magnetic dipoles due to presence of unpaired electrons (circulating charges also result in magnetic dipoles). Sometimes we are also interested in nuclear magnetism which can be explained by nucleons present in the nucleus of the system. In most of the cases, magnetic moments due to the nuclei become insignificant because magnetic moments of the nuclei are smaller than the magnetic moments of electrons by a factor of 10^{-3}. Thus, the magnetic moment of a free atom has three major sources of magnetism: (i) the spin with which electrons are endowed; (ii) the change in the electron orbital moment provoked by an externally applied magnetic field; and (iii) their orbital angular momentum about the nucleus [Kittel (1996)]. The magnetic moment associated with spinning motion and motion in orbit is a vector quantity used to determine the tendency of an atom to interact through an external magnetic field, normal to the plane of the orbit and parallel to the axis of the spin, respectively. The magnetic moment of an atom is a vector sum of all its electronic moments and moments arising due to various possibilities leading to a variety of magnetic classes such as diamagnetism, paramagnetism, ferromagnetism, antiferromagnetism, and ferrimagnetism.

1.4.1. Theory of Diamagnetism

Diamagnetism is a characteristic behavior of all matters. The diamagnetism is a materials property that displays negative magnetism. Although it is composed of atoms which have no net magnetic moment in the absence of magnetic field, it reacts in a particular fashion to an applied magnetic field. When a diamagnetic substance is kept in an external magnetic field, a feeble magnetic dipole moment is stimulated in the opposite direction to the applied magnetic field according to the Lenz's law so that both

the magnetization and the susceptibility are negative. The classical theory of this effect was first carried out by Paul Langevin, a French physicist [Langevin (1905)]. Electrons which form a closed shell in an atom around nucleus typically have their orbital and spin moments oriented such that the atom as a whole has no net magnetic moment. Bismuth (Bi), mercury (Hg), gold (Au), copper (Cu) are some examples of diamagnetic materials. A magnetic material subjected to the magnetic field, can increase or decrease the magnetic flux density. Diamagnetic substances diminish the density of the lines of magnetic forces, and this effect is produced by the movement of electrons in the atoms. Usually, for the diamagnetic substances, magnetic susceptibility is negative ($\chi < 0$) and it is independent of the temperature. Superconductors in which electrons make cooper pairs are perfect diamagnets with $\chi = -1$.

1.4.2. Theory of Paramagnetism

Diamagnetism is an intrinsic characteristic of all matters, but the presence of other types of magnetism is a result of the fact that many atoms have a permanent magnetic dipole moment which overbalances the diamagnetic effect. In some substances, the permanent magnetic dipole moments of the atoms have no mutual interaction between them; this effect is known as paramagnetism. However, in the presence of an external magnetic field, the magnetic moments of a paramagnetic (PM) substance have the tendency to rotate themselves along the magnetic field. In the absence of any opposing force, a complete alignment of the magnetic moments will be achieved, and the substance would acquire a large magnetization in the same direction of the magnetic field, however thermal agitation tries to keep the magnetic dipole moments at random and it results in only a partial alignment of the moment in the direction of field. Effectively materials with atoms of unpaired electron spins are PM. The magnetization or susceptibility of a PM substance decreases with increasing

temperature and follows Curie's law, i.e., $\chi = C/T$, where, C is Curie constant and T is absolute temperature.

1.4.3. Theory of Ferromagnetism

In contrast to the diamagnetic and paramagnetic substances, ferromagnetic (FM) substances exhibit spontaneous magnetization (M_0) even in the absence of an external magnetic field. Hence, ferromagnetism is defined as the presence of large spontaneous magnetization, whose orientation can be switched by the application of an external magnetic field. The origin of the spontaneous magnetization is due to an internal 'molecular field' which tends to line up the magnetic dipole moments of the substance parallel [Cullity (1972)]. The origin of the molecular field is quantum mechanical exchange energy, which results in parallel spins for the electrons (and consequently parallel magnetic moments) to have minimum energy than electrons with anti-parallel spins in the FM materials. When FM substances are heated, the degree of parallel alignment of the atomic magnetic moments reduces due to thermal agitation, i.e. it becomes disordered, and the FM materials transform to PM at higher temperatures. The temperature at which FM to PM transition takes place is known as the Curie-temperature (T_C). The saturation magnetization goes to zero at the Curie temperature. Above T_C the susceptibility varies according to the Curie-Weiss law given by the equation (1.2):

$$\chi = \frac{C}{T - T_C} \tag{1.2}$$

The as-prepared samples of ferromagnetic materials frequently lack a macroscopic magnetization because of the presence of domains of magnetization oriented in various directions to minimize the energy of the system. The succeeding reorientation and alignment of the domains, on the application of an external magnetic field (H), results in a hysteresis in the magnetization (M) and the externally applied

magnetic field (H) [Hill et al. (2000)]. **Fig. 1.2** shows a typical magnetic hysteresis between magnetization and magnetic field.

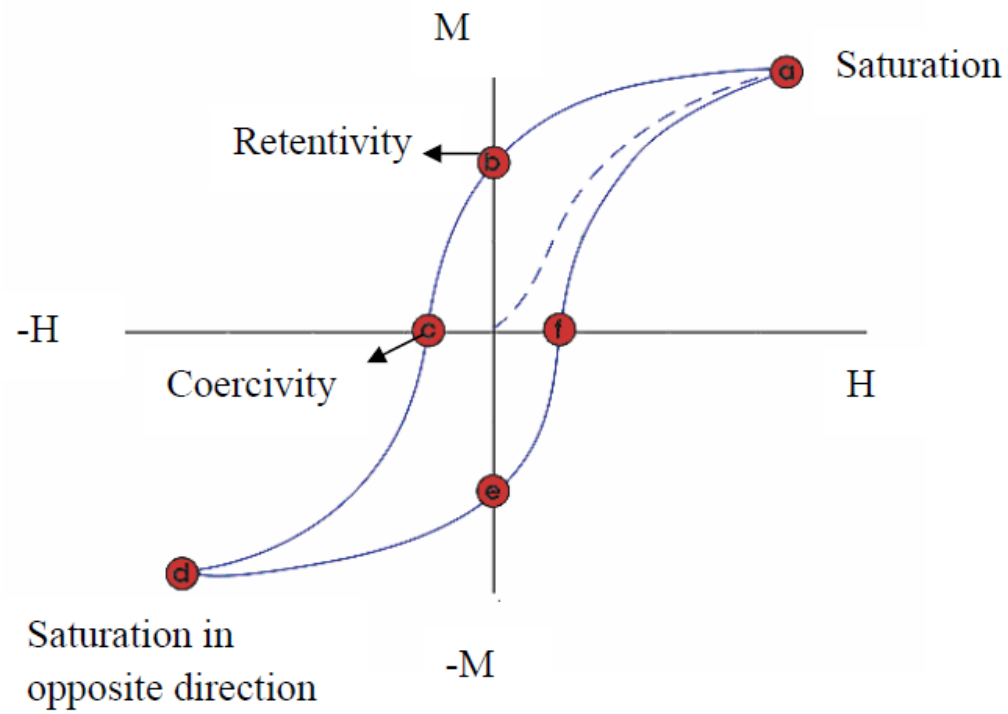

Figure 1.2: Typical magnetic hysteresis loop (M-H) for ferromagnetic materials [after Cullity (1972)].

1.4.4. Theory of Antiferromagnetism

When the alignment of the spin moments of neighboring atoms is antiparallel to each other, it is termed as antiferromagnetism. The exchange interaction, in this case, favors antiparallel alignment of the spins. So, we can assume two sublattices say A and B in which magnetic moments are aligning themselves in the antiparallel direction (up-down) to each other. In this situation, no net magnetic moment is associated with the system, because there is a complete cancellation of both orbital and spin magnetic moments.

There are several manners of arranging an identical number of up and down spins depending on the type of crystal lattice on which the spins are to be placed. These arrangements of spins result in different types of antiferromagnetic (AFM) ordering such as A, C, G, or E-type as shown in **Fig. 1.3**. The AFM ordering disappears above a critical temperature recognized as the Neel-temperature (T_N). Above T_N, the material behaves like a typical paramagnet. Below T_N, due to lower thermal energy as compared to the gain due to the antiparallel ordering of neighboring spins, the antiferromagnetic state is formed. A plot between the inverse of susceptibility (χ^{-1}) and temperature (T) gives a straight line for antiferromagnets also, just like ferromagnets above T_N but this line extrapolates to negative Curie-temperature (T_C) at $\chi^{-1} = 0$. Above T_N, they obey the Curie-Weiss law with negative T_C. Although, one does not expect net magnetization in the AFM materials, but, it may exhibit net magnetization due to spin canting, lattice defects and frustrated surface spins in the absence of external magnetic field. At sufficiently high magnetic fields, the spin direction of one of the magnetic sublattice may rotate and eventually lead to the 'spin-flop' where all the spins would be aligned in a parallel fashion. Because of this rotation and spin-flop, magnetization can be induced by an external magnetic field.

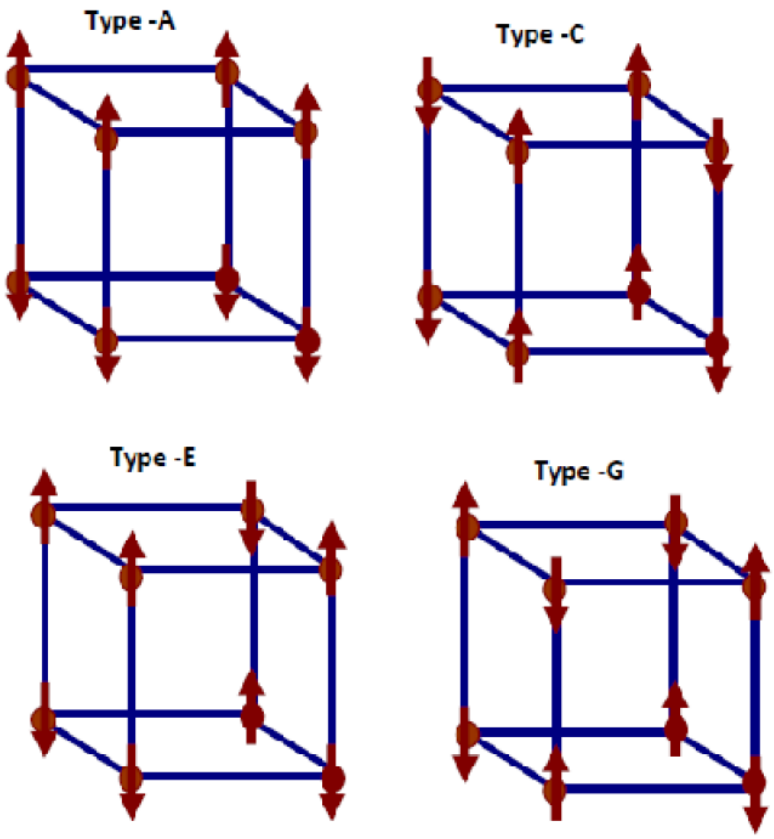

Figure 1.3: Different types of magnetic lattice arrangements resulting in different type (A, C, G and E-type) antiferromagnetic ordering [drawn using the convention of Wollen et al. (1955)].

1.4.5. Theory of Ferrimagnetism

Ferrimagnetic materials exhibit a considerable M_0 at room temperature, just similar to ferromagnetic substances, and this fact only makes them technologically important. Like FM, they consist of magnetically saturated domains, and they display the phenomena of magnetic hysteresis and saturation. Their M_0 vanishes above Curie-temperature. In ferrimagnetic substances, there are also two sublattices A and B, just similar to AFM, but in this case, only partial cancellation of magnetic moments of A and B sublattices takes place. The most important ferrimagnetic substances are certain double oxides of iron and other metals, called ferrites (although all ferrite oxides are not FM). The ferrimagnetics were not recognized as forming a distinct magnetic class until

1948. A classic paper by L. Neel et al. (1948) provided the theoretical explanation to an appreciative of the ferrites and the word ferrimagnetism has come due to him.

The temperature dependence of variation in the inverse of magnetic susceptibility (χ^{-1}) and saturation magnetization (M_s or σ_s) for different types of magnetic materials are shown in **Fig. 1.4**.

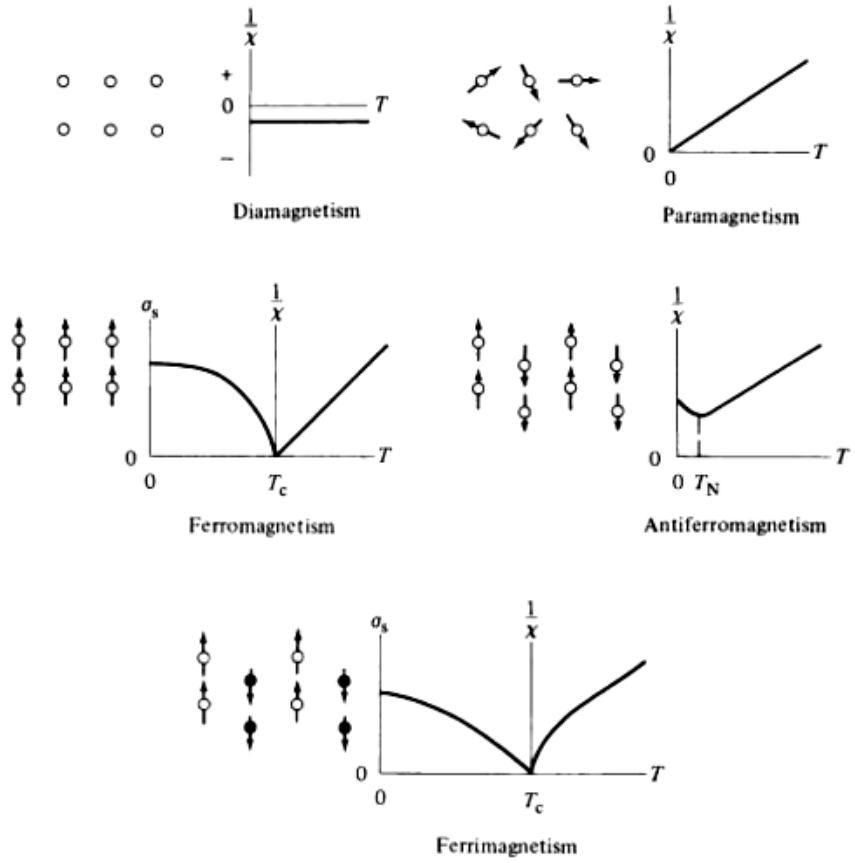

Figure 1.4: Schematic presentation of saturation magnetization (M_s or σ_s) and the inverse magnetic susceptibility (χ^{-1}) for diamagnetic, paramagnetic, ferromagnetic antiferromagnetic and ferrimagnetic substances [after Cullity et al. (2008)].

1.5. Magnetic Interactions

Quantum mechanical exchange interactions are responsible for the phenomenon of long-range magnetic ordering in magnetic materials. The coupling of the magnetic

moments, which is quantum mechanical in nature occurs between identical particles, is called as exchange interaction and is necessarily an outcome of overlapping of electronic orbitals keeping in mind Pauli's exclusion principle. Exchange interactions are in some sense like electrostatic interactions, resulting since charges having the same sign cost energy when they are very close to each other and save energy when they are separate from each other. We discuss below the different types of exchange interactions which lead to the long-range magnetic ordered state.

1.5.1. Direct Exchange Interaction

In condensed matter physics, the phenomenon of exchange interactions is a quantum mechanical effect which occurs in identical particles. When the electrons on neighboring magnetic ions are sufficiently close to have enough overlap of their wave functions, they interact through exchange interaction. This type of interaction is identified as a direct exchange. It results in a strong short-range coupling, which diminishes quickly on increasing the separation between the magnetic ions. For direct exchange interaction, the exchange integral (J_{ex}) can be negative or positive depending on the equilibrium between kinetic and coulombic energies. In the framework of the Ising model, exchange energy is given by Equation (1.3) [Cullity (1972)]:

$$E_{ex} = -J_{ex}\, S_i.S_j \qquad (1.3)$$

Where, E_{ex} is the exchange energy, S_i and S_j are the electronic spins at the i and j^{th} atomic sites which can take values +1/2 or -1/2. Thus, for two atoms having single electron each, when they are very close to one another the coloumbic interaction is minimal and the electrons spend most of their time in between the nuclei. Since the electrons are then required to be present at the same position in space at the same time, then according to Pauli's exclusion principle, it is necessary for them to possess antiparallel spins. This gives rise to antiparallel alignment, i.e. AFM ordering and

therefore negative exchange interaction J_{ex} as given in Equation (1.3). But, if the atoms are so far apart, then the electrons spend their time away from each other to reduce the electron-electron coulombic interaction. This can give rise to a parallel alignment of the spins, i.e. FM ordering with positive exchange interaction. The nature of direct exchange interaction can be determined using the Bethe-Slater curve as shown in **Fig. 1.5** which demonstrates the magnitude and sign of exchange integral (J_{ex}) as a function of inter-atomic distance.

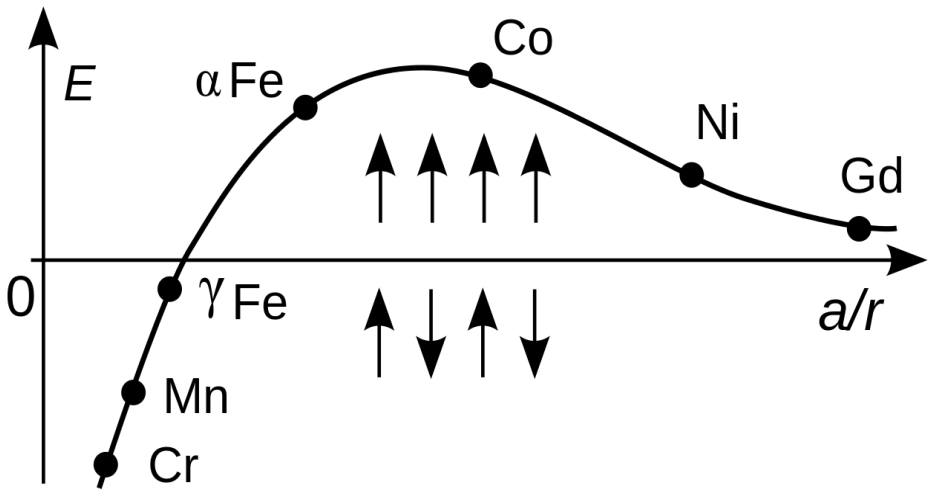

Figure 1.5: Schematic representation of Bathe-Slater curve, here, 'a' is the atomic radius and r is the radius of its 3d orbital where electrons are present [after Cullity (1972)].

1.5.2. Indirect Exchange Interaction

The conduction electrons can also mediate the magnetic interactions among magnetic ions. A confined magnetic moment, spin-polarizes the conduction electrons and this polarization in turn couples to an adjacent confined magnetic moment at a distance 'r'. The nature of this exchange interaction is of an indirect type because it does not hold direct coupling among the magnetic moments. This type of interaction is commonly known as Ruderman-Kittel-Kasua-Yoshida (RKKY) interaction (or also as

itinerant exchange interaction) [Ruderman et al. (1954); Kasuya et al. (1956); Yosida et al. (1957)], named after the discoveries of the effect. The RKKY type exchange coupling $J_{RKKY}(r)$ is given by Equation (1.4):

$$J_{RKKY}(r) \propto \cos(2k_F r)/r^3 \qquad (1.4)$$

at a large r (considering a spherical Fermi surface of radius k_F) [Blundel et al. (2001)]. The RKKY interaction shown in **Fig. 1.6** is long ranged and has a damped oscillatory (oscillates between positive and negative values) dependence on the separation between the magnetic moments. Therefore, depending upon the separation among a pair of magnetic ions, the coupling between them can be of FM or AFM nature.

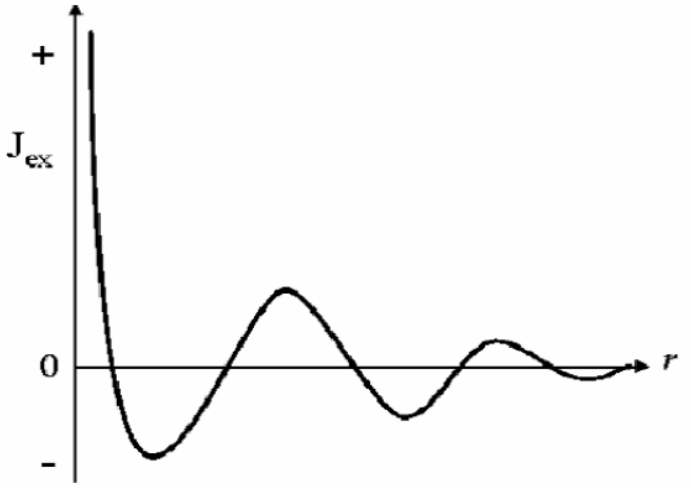

Figure 1.6: The coefficient of RKKY versus the inter-atomic distance r [after Rutheman et al. (1954)].

1.5.3. Superexchange Interaction

Superexchange interaction illustrates the interaction among moments of ions which are too far apart to be influenced by direct exchange, but are coupled over a comparatively long distance via a non-magnetic ion which is located in between the magnetic ions [Anderson (1950)]. For example, MnF_2 and MnO are both

antiferromagnets. However there is no direct overlap among the electronic wave functions of Mn^{2+} ions in each system. If the system is completely ionic, each metal ion would have a single unpaired electron in a d-orbital whereas oxygen has 2p electrons in its outer most occupied states. The strength of the antiparallel coupling among metal ions (M) depends on the bond angle M-O-M and it is usually highest when this angle is 180^o i.e. when the spins are collinear.

1.5.4. Double Exchange Interaction

In several oxides, it is probable to have an FM exchange interaction due to the occurrence of magnetic ions showing mixed valency, i.e. it can exist in more than one oxidation states. For example, Manganese ion can exist in +3 and +4 oxidation states, i.e. as Mn^{3+} and Mn^{4+}, in the mixed-valence manganite system such as $La_{1-x}Ba_xMnO_3$. The FM alignment in such systems is governed by the double exchange (DE) mechanism [Zener (1951)] and can be understood considering **Fig. 1.7**. In the case of mixed valency of Mn ions, e_g electron on Mn^{3+} ion can hop to a neighboring site of Mn^{4+} via oxygen by interacting with 2p electrons of O^{2-}. This is possible only if there is a vacancy of the same spin. However, due to the strong Hund's coupling, the three electrons in the t_{2g} level want to keep the e_g electron aligned to them. Thus it is not energetically favorable for an e_g electron to hop to an adjacent ion where the t_{2g} spins will be antiparallel to the e_g electron. FM alignment of neighboring ions is required to preserve the high-spin arrangement on both the receiving and the donating ions. This model is alike to superexchange. In superexchange, an AFM or an FM alignment takes place among two atoms with the same number of electrons (valence), while in double exchange; the interaction takes place only when one atom has an extra number of electrons compared to the other.

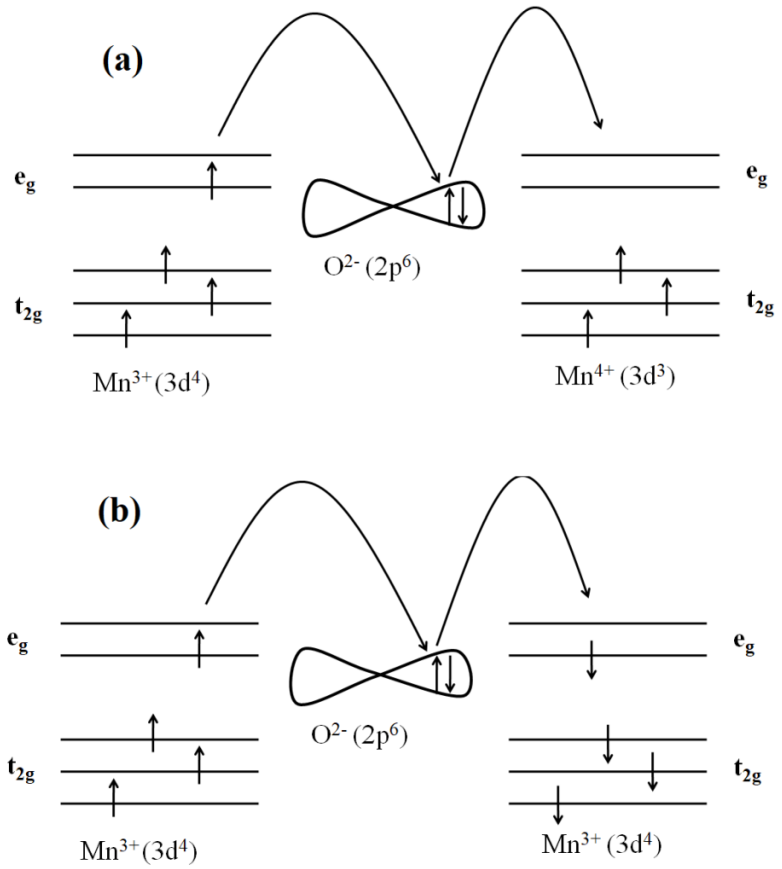

Figure 1.7: Schematic representation of (a) DE interaction among Mn^{4+} and Mn^{3+} cations and (b) SE interaction among Mn^{3+} and Mn^{3+} cations through O^{2-} anion [Zener (1951)].

1.6. Crystal Field Splitting and Jahn-Teller Distortion

The physical properties in the perovskite manganites in the form of $AMnO_3$ (A being rare earth elements) are largely decided by MnO_6 octahedra, which forms a basic building block in this structure. In **Fig. 1.1** schematic perovskite structure is depicted. Usually in isolated manganese atom, five orbitals of d-level are degenerate but when the Mn-ion is surrounded by six oxygens in regular octahedral environment of crystal, degeneracy is lifted. The five levels get split into two groups with energy difference Δ_{oct} (= 1 to 2 eV), the lower triplet t_{2g} and upper doublet e_g. This occurs due to the electrostatic interaction between the d-electrons of Mn ions and surrounding negative

ligand ions (oxygen). The doubly degenerate e_g molecular orbitals ($d_{x^2-y^2}$ and $d_{3z^2-r^2}$) point in the directions where the negatively charged oxygen ions are situated thus enhances the energy due to coulombic repulsion. On the other hand, triply degenerate t_{2g} molecular orbitals (d_{xy}, d_{yz}, and d_{zx}) point in the directions between the ligands where fields are less, and therefore stabilize in lower energy. This situation is schematically depicted in **Fig. 1.8. A**s the consecutive electrons are introduced in d-shell of Mn-ion, they occupy the lowest available Mn-ion orbitals, compatible with total spin associated with the ions of Mn^{3+} and Mn^{4+}, so their electronic configurations are $t_{2g}^3e_g^1$ and $t_{2g}^3e_g^0$, respectively.

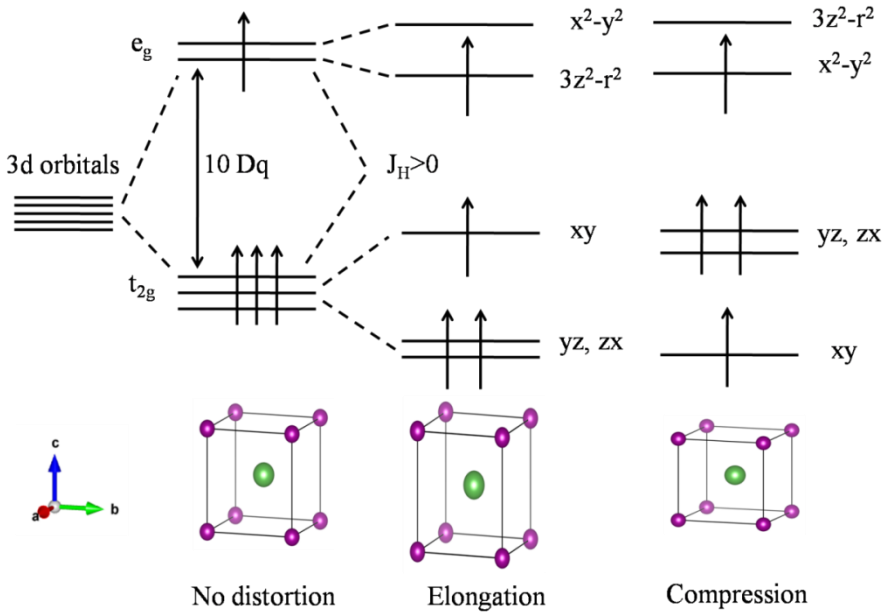

Figure 1.8: Crystal-field splitting of the five-fold degenerate atomic 3d levels into higher e_g (doubly degenerate) and lower t_{2g} (triply degenerate) levels. The JT distortion of the octahedron of MnO_6 further lifts each-degeneracy [after Tokura (2006)].

As discussed above, the crystal field effect leads to splitting in d-orbitals into an e_g doubly degenerate and t_{2g} triply degenerate, the remaining degeneracy is further lifted by Jahn-Teller (JT) distortion [Jahn and Teller (1937)]. JT showed that, if the electronic state of a non-linear molecule is orbitally degenerate, then there always exists at least one vibrational coordinate along which the molecule may go under distortion to lower

its energy and hence stabilization. The situation can be exemplified for Mn^{3+} ion. The presence of a single electron in doubly degenerate e_g orbitals can distort the octahedra where the surrounding oxygen atoms can slightly readjust their positions, generating an asymmetry in different directions that effectively gets rid of the degeneracy. This is known as JT distortion which is found to have a crucial role in stabilizing various phases in perovskite manganites. The octahedra MnO_6 are distorted in such a way that the center of gravity of the e_g levels and that of the t_{2g} levels is unaffected. This is manifested in the form of Basel planes distortion with one diagonally opposite oxygen pair displaced outwards, and other pair displaced inside, or Basel plane oxygens displaced inside, and apical oxygens displaced outside. This distortion can be static as observed in small hole-doped manganites, or dynamic that is a given ion is not frozen in one distorted arrangement and evolves between different arrangements as a function of time. However, this distortion splits e_g band opening a gap in Fermi level.

1.7. Complex Ordering in Perovskite Manganites

Due to strong correlation effect, electrons which are normally localized at specific atomic sites, often display cooperative electronic ordering phenomena, such as spin order, charge order and orbital order in the perovskite manganites [Tokura (2006), Rao et al. (2000)]. These novel quantum collective properties are generally accompanied by concomitant structural, magnetic and metal-insulator phase transitions and so forth. Thus they are believed to play important roles in controlling these attractive physical properties.

1.7.1. Charge Ordering

The physics of perovskite manganites has been studied rigorously in recent years consequent upon the discovery of CMR in lots of compositions of the doped $LaMnO_3$ manganite. These compounds display various unique ranges of couplings between Mn-

electron spin, charge and orbital degrees of freedom. It is now well established that numerous ground states are possible for doped manganites, primarily the itinerant FM and insulating charge-ordered (CO) AFM states, and these often coexist over a range of length scales. The CO state in doped manganites is described by an ordering of Mn^{4+} and Mn^{3+} cations within the MnO_2 plane, causing the localization of e_g electrons and the AFM spin ordering below the CO transition temperature (T_{CO}) [Zhang et al. (2007)]. The signature of the charge ordered (CO) ground state is most easily examined in half-doped manganites, e.g., $La_{0.5}Ca_{0.5}MnO_3$. The theoretical model for this CO state was suggested by Goodenough (1955) after the magnetic structure was observed to be multifaceted CE-type FM couplings along zig-zag chains. The CO phenomenon is one of the fascinating issues in these substances because of the strong interactions between the spin, charge, orbital and lattice degrees of freedom and has been studied intensively. The CO states are novel demonstrations arising from the interaction between the phonons and the charge carriers. Charge ordering arises as the charge carriers are localized into some specific sites below T_{CO}, giving rise to long-range order all through the crystal structure.

1.7.2. Orbital Ordering

Orbital ordering (OO) in perovskite manganites occurs at certain carrier concentrations when d-electrons occupy an asymmetric molecular orbital. The driving force is partially direct electrostatic repulsion of the charge clouds but coupled JT distortions of neighboring octahedral stabilizes the effect. Goodenough (1955) proposed a comprehensive qualitative understanding of the OO; he suggested that this ordering would involve displacements of the $Mn^{4+}O_6$ octahedra along [101] direction. Radaelli et al. (1997) studied OO in half-doped $La_{0.5}Ca_{0.5}MnO_3$ manganite, and they reported that the development of magnetic ordering is correlated with the emergence of weak

reflections in X-ray diffraction patterns, which are the indication of small structural distortions because of orbital and charge ordering. It was found that, in agreement with Goodenough's assumption, the superstructure (a quasicommensurate) is described by a large JT distortion of the $Mn^{3+}O_6$ octahedra, whereas the $Mn^{4+}O_6$ octahedra stay almost undistorted [Radaelli (1997)]. Additionally, OO occurs due to the displacement of the $Mn^{4+}O_6$ octahedra mostly along [001] direction which is not consistent with Goodenough's early postulations. The e_g-orbitals ($d_{3z^2-r^2}$) of $Mn^{3+}$and the associated lattice distortions (long Mn-O bonds) also establish long-range order, causing to orbital ordering. Thus, at low temperatures, the rare-earth perovskite manganites are AFM ordered with CE or A-type ordering, but only the earlier occurs in the charge-ordered systems where the e_g electrons are localized. The CE-type spin ordering is characterized by the ordering of Mn^{4+} and Mn^{3+} ions alternately.

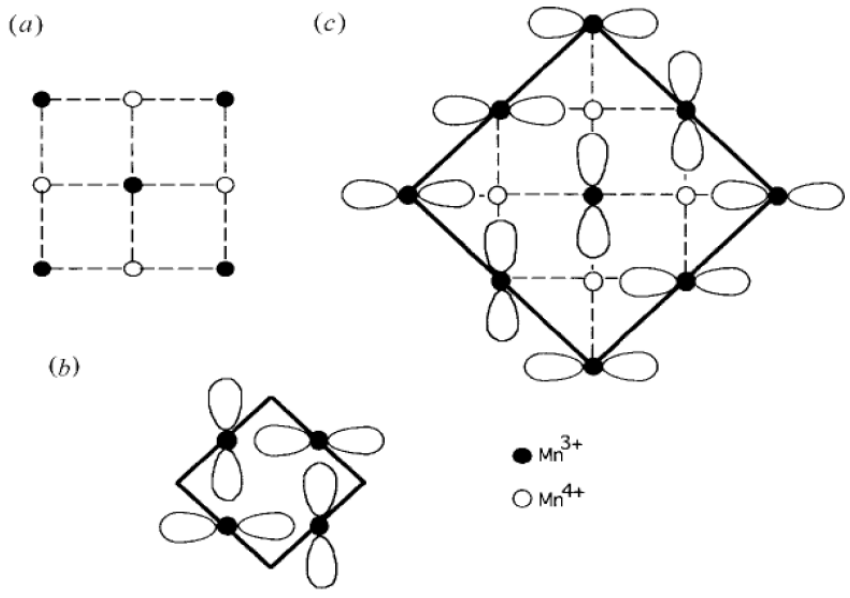

Figure 1.9: (a) Diagram showing charge ordering of Mn^{4+} and Mn^{3+} cations in a mixed-valence manganite ($R_{1-x}A_xMnO_3$) with x = 0.5, (b) Orbital ordering of the $d_{3z^2-r^2}$ orbitals of Mn^{3+} with x = 0, (c) collective charge and orbital orderings for x = 0.5 [after Rao et al. (2000)].

1.8. Magnetoresistance (MR)

Nowadays, the magnetoresistive (MR) effect is a very attractive research topic in both fundamental and applied physics point of views. Their significance was initially related to technological applications mostly in magnetic data storage and magnetic recording. Quickly, it was observed that it is adequately important to study these phenomena in detail from an exclusively scientific point of view. MR is defined as the relative change in the electrical resistivity of a substance under the application of a magnetic field. Mathematically, it can be expressed by Equation (1.5):

$$\mathrm{MR(H)} = \frac{\rho(\mathrm{H})-\rho(0)}{\rho(0)} \tag{1.5}$$

Where, $\rho(0)$ and $\rho(H)$ are resistivity of the substance in the absence and presence of the magnetic field, respectively. Depending on the relative change in the electrical resistivity on the application of magnetic field, it is called either as Giant magnetoresistance (GMR) or Colossal magnetoresistance (CMR) [Tokura (2006)].

1.8.1. Colossal Magnetoresistance (CMR)

Colossal magnetoresistance (CMR) is a property of few materials, typically mixed-valence perovskite manganites that makes possible them to significantly modify their electrical resistivity in the presence of a magnetic field. Initially, it was discovered by G. H. Jonker and J. H. van Santen [Jonker and Santen (1950)] in the 1950s in $La_{1-x}A_xMnO_3$ (A = Ca, Sr, Ba) mixed-valence manganites. In the early 1990s, a new kind of CMR was rediscovered in the thin films based mixed-valence manganites by Jin et al. (1993) and Helmolt et al. (1994). The electrical transport comprises perhaps the most beautiful physical property of CMR manganites. The physics of CMR in manganites is decided by the strength of spin interactions which is strongly dependent on the doping concentration and the temperature. At room temperature, $Nd_{1-x}Sr_xMnO_3$ shows the FM ordering for $0.3 < x < 0.5$. When doping level is increased further, the

compound shows the A-type AFM ordering for $0.5 < x < 0.7$ closely connected to the bad metal characteristics which are widely detected in the conducting transition-metal oxides exhibiting strong electron-electron and electron-lattice correlations. The correlated electrons, which are nearly localized on their atomic sites, bear three features, that is, orbital, charge and spin degrees of freedom. Due to JT interaction, the conduction electrons with an orbital degree of freedom are scattered not just by the strong electron correlation/spin correlation effect but also through the strong lattice-electron coupling. The local or collective JT distortions, as explained by the movement of the oxygen ions in the MnO_6 octahedra, are observed universally when the system displays the remarkable change in resistivity (e.g., insulator to metal) or magnetic transitions (e.g., AFM to FM) [Tokura (2006)]. The possibility of phase separation or phase inhomogeneity has commonly been argued as the important feature in CMR physics [Dagotto (2005)]. **Fig. 1.10** shows the evolution of electrical resistivity in $La_{2/3}Ca_{1/3}MnO_3$ manganite as the function of temperature and magnetic field.

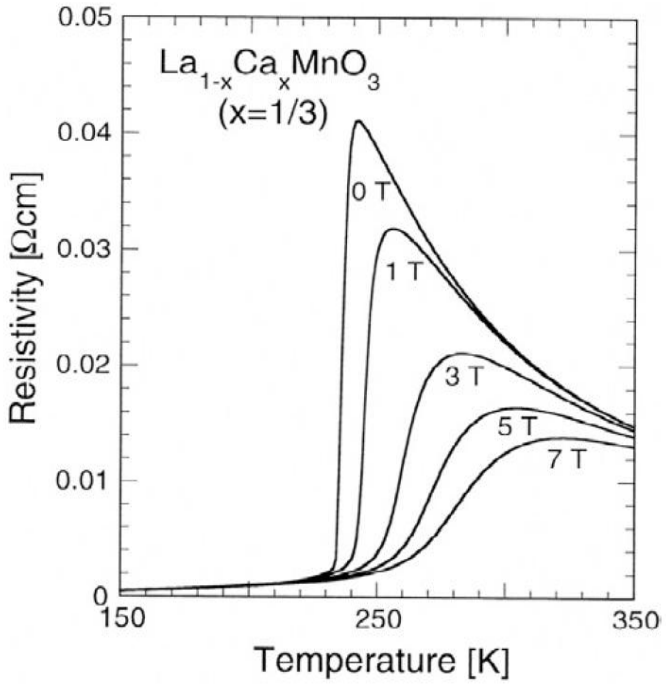

Figure 1.10: Colossal magnetoresistance (CMR) behavior for the $La_{2/3}Ca_{1/3}MnO_3$ single crystal [after Tokura (2006)].

1.8.2. Giant Magnetoresistance (GMR)

Approximately equivalent to the study of the phenomenon of fundamental CMR, a new variety of magnetoresistance (MR) was found out in granular manganite samples known as giant magnetoresistance **(**GMR). This effect is not detected in single crystals and was quickly related to spin-polarized tunneling among the adjacent grains. Therefore, it is typically denoted as intergranular MR (IMR) [Baibich et al. (1988)]. There are large similarities among this MR and the previously studied one in FM/metal and FM/insulator alloys; however, the MR values observed in these situations are much higher. The important explanation of this IMR lies once more in the inherent properties of the manganites, achieved from their particular electronic configuration [Binasch et al. (1989)]. In general, in an FM material, the band structure is spin-dependent, and two sub-bands are found for the minority (spin antiparallel to magnetization), and the majority (spin parallel to magnetization) spins. Consequently, a net spin polarization (P) occurs. In perovskite manganites, there exists an energy gap (~ 1 eV) in the density of states of the minority carriers, and so the total spin polarization is unity. In the spin tunneling representation, GMR depends significantly on the spin polarization, and thus the higher spin polarization values in manganites result to higher values of MR than those observed for other FM alloys [Baibich et al. (1988)].

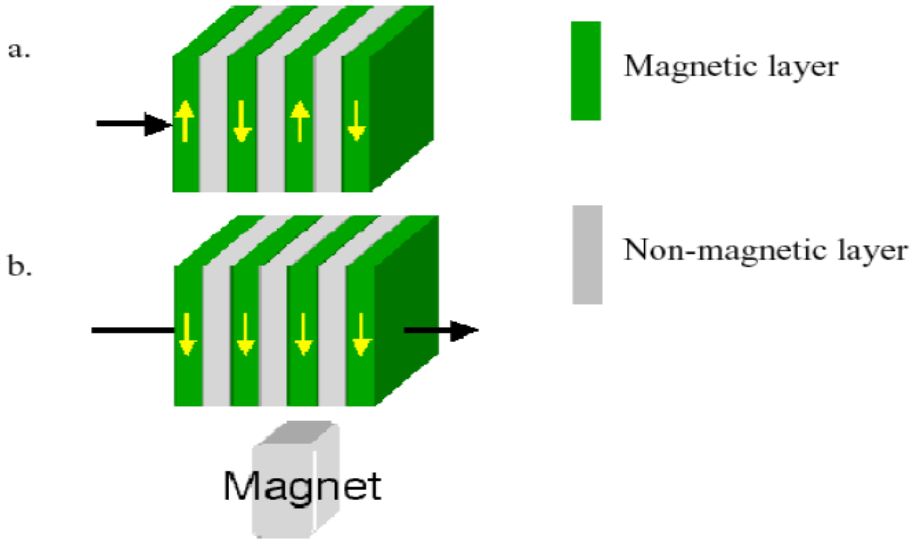

Figure 1.11: GMR materials are prepared from alternate layers of magnetic and non-magnetic metals having the thickness in nanometers scale; (a) antiferromagnetic and (b) ferromagnetic spin arrangement [drawn using the convention of Binasch et al. (1989)].

1.9. Review of Crystal Structure and Magnetic Behaviors in Mixed-Valence Perovskite Manganites

The complex interaction among spin, charge, orbital and phase separation degrees of freedom and their responsibility on magnetic state and phase transition properties of rare-earth mixed-valence perovskite manganites ($R_{1-x}A_xMnO_3$; R = rare-earth trivalent cations and A = divalent alkaline earth cations) have made them very attractive for scientists and researchers from several decades [Coey (2004); Levy et al. (2000); Park et al. (2006); Kawano et al. (1996)]. In recent times, crystallite size and Mn-site substitution have been revealed to be the two other very significant factors which can influence the magnetic state and phase transition properties of the mixed-valence manganites [Shankar et al. (2015); Nam et al. (2006)]. It is recently observed in rare-earth mixed-valence manganites that when the particle size is reduced to the nanoscale, the low-temperature orbital and charge ordered insulating phase is

destabilized due to suppression of charge ordering transition and stabilization of high-temperature FM metallic state [Rao (2000); Kundu et al. (2012)]. From few years researchers are working on the Mn-site substituted manganite systems. Ganguly et al. studied effects of substitution of ruthenium and chromium for manganese on the magnetic and transport properties of electron-doped $Ca_{0.9}Ce_{0.1}MnO_3$ manganite, with d_z^2 orbital-ordered and the correlated AFM characters [Ganguly et al. (2002)]. They reported that the substitution of chromium and ruthenium suppresses AFM transition. Dho et al. also studied the effect of chromium doping on magnetic properties of $La_{0.46}Sr_{0.54}Mn_{1-x}Cr_xO_3$ ($0 \leq x \leq 0.08$) and found that FM to AFM transition vanished for $x = 0.08$ due to the appearance of FM-DE interaction among Mn^{3+} and Cr^{3+} ions [Dho et al. (2002)]. The effect of non-magnetic Ti^{4+}-ions substitution on structure, magnetic and transport behaviors of $La_{0.7}Sr_{0.3}Mn_{1-x}Ti_xO_3$ ($0 \leq x \leq 0.5$; LSMTO) films made by chemical solution deposition was studied by Zhu et al. (2006). They found that lattice constant increases with increasing Ti^{4+} concentrations up to $x = 0.3$ due to replacement of Mn^{4+}-ions ($r = 0.530$ Å) by Ti^{4+}-ions ($r = 0.605$ Å) and after that it start decreasing due to substitution of Mn^{3+}-ions ($r = 0.645$ Å) by Ti^{4+}-ions ($r = 0.605$ Å) in the lattice. The magnetic study of LSMTO shows that FM component decreases and AFM contribution increases with enhancing Ti-doping concentration. Magnetoresistance (MR) study reveals that MR increases near Curie-temperature on the increase of Ti^{4+} content at Mn-site.

1.9.1. Electrical and Magnetic Phase Transitions in $Nd_{1-x}Ba_xMnO_3$ Manganites

The $Nd_{1-x}Ba_xMnO_3$ (NBMO) manganites have not been given much attention due to its very low magnetic transition temperature. Many researchers and scientists studied NBMO, but they did not investigate this system in more detail. First-time Troyanchuk et al. (1999) studied NBMO manganite and presented the magnetic phase

diagram for this. **Fig. 1.12** shows the magnetic phase diagram for NBMO ($0 \leq x \leq 0.44$). They reported that NBMO exhibits inhomogeneous AFM behavior for the compositions in the range $0 \leq x \leq 0.05$; a mixed AFM-FM state for $0.05 < x < 0.10$; FM with antiferromagnetic clusters for $0.10 < x < 0.20$, a pure long-range FM state in the compositions range $0.2 \leq x < 0.4$ and for $x > 0.4$ an inhomogeneous FM state is observed. Further, they found a Metal-like behavior below Curie-temperature (T_C) for the compositions $0.3 < x \leq 0.44$. The value of T_C increases with increasing concentration of Ba^{2+} ion up to 0.34 ($T_C \sim 145$ K) and above $x = 0.34$ the value of T_C further start decreasing [Troyanchuk et al. (1999)].

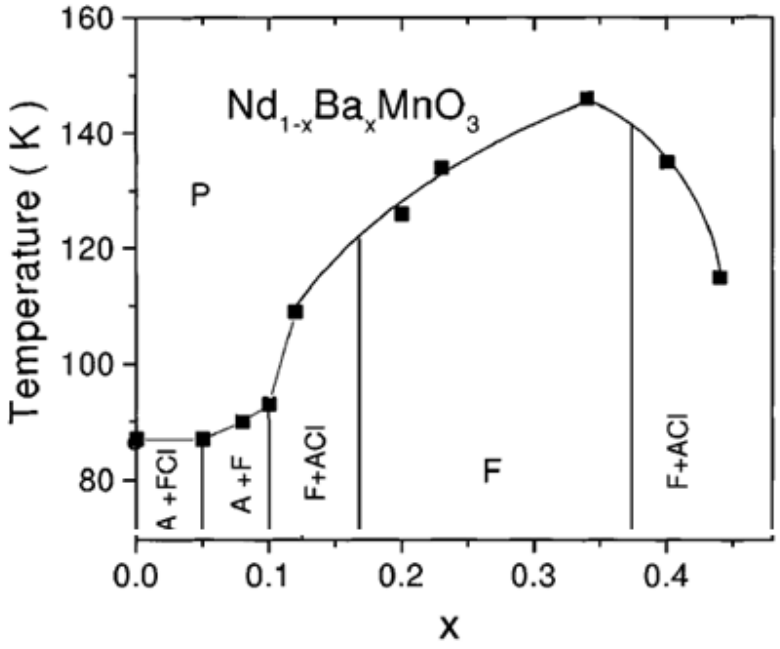

Figure 1.12: Magnetic phase diagrams for $Nd_{1-x}Ba_xMnO_3$ manganites series. F = ferromagnet, A = weak ferromagnet, ACl = antiferromagnetic clusters, FCl = ferromagnetic clusters [after Troyanchuk et al. (1999)].

After 12 years of Troyanchuk et al., in 2002, Trukhanov et al. reinvestigated the electrical and magnetic properties of $Nd_{1-x}Ba_xMnO_3$ manganites, and they also found a similar magnetic phase diagram as reported earlier along with semiconducting behavior [Trukhanov et al. (2002)]. They prepared two sets of samples one in the presence of air and another in the presence of a reduced atmosphere (Ar + CO). They found that the value of T_C for reduced samples increases from very low temperature to near room-temperature. **Fig. 1.13** displayed magnetic phase diagram along with electrical behavior for NBMO manganites.

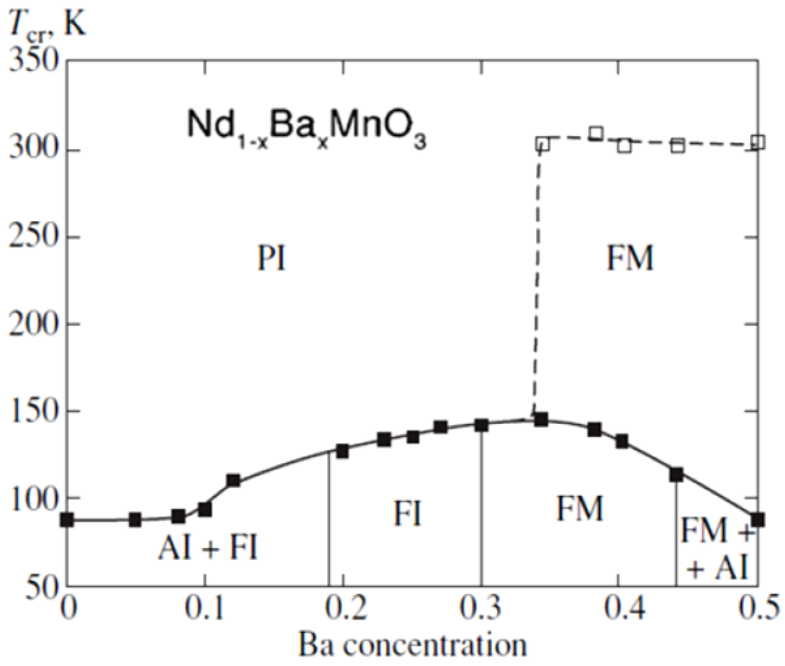

Figure 1.13: The magnetic phase diagram along with electrical behavior for polycrystalline samples of two $Nd_{1-x}Ba_xMnO_{3-\delta}$ manganites. Solid symbols show the sample prepared in the air, and that synthesized in a reducing medium, by hollow symbols. AI = AFM semiconductor, FI = FM semiconductor, FM = FM metal and PI = PM semiconductor [after Trukhanov et al. (2002)].

1.9.1.1. Structural, Magnetization and Electrical Resistivity of $Nd_{0.7}Ba_{0.3}MnO_3$ Manganite

Wang et al. (2000) studied structural, magnetoresistive and magnetic transitions in $Nd_{0.7}Ba_{0.3}MnO_3$ (NBMO-30) manganite. They reported that the powder XRD profiles could be indexed with a pseudo-tetragonal or orthorhombic ($a \approx b \geq c/2^{1/2}$) structure with a = 5.508(1) Å, b = 5.496(2) Å and c = 7.764(3) Å. They did not clearly discuss about the space group of the orthorhombic structure. The compound NBMO-30 displays two magnetic transitions; first PM to FM transition at T_C = 115 K and second the partial ordering of the Nd moments around T_{Nd} ~ 40 K. They have presented experimental proofs that the magnetic phase in the low-temperature region contains the Nd moments, and that are aligned partially parallel or parallel to the ferromagnetically ordered Mn moments. Wang et al. (2000) recorded resistance of the NBMO-30 manganite in the presence of magnetic field of 9 T and in the absence of magnetic field and observed a large MR of 90%-98% over the whole temperature range T < 120 K along with the maximum MR of ~98% at 95 K, near PM to FM phase transition. The large MR persisting down to the lowest temperature should be strongly related to the existence of the low-temperature magnetic phase below T_{Nd} in NBM0-30 manganite. Roy et al. (2008) reported the effect of particle/crystallite size on structural, magnetic and electrical behaviors of NBMO-30 manganite in more detailed. They synthesized nanoparticles (NPs) of NBMO-30 of various particle sizes (20, 25, 33 and 41 nm) using sol-gel technique and studied its structural, magnetic and electrical properties. **Fig. 1.14** shows room temperature (RT) XRD patterns for the nanoparticles of NBMO-30 manganite of particle sizes 20, 25 and 41 nm and inset display Rietveld refined fit for NBMO-30 sample with a particle size 33 nm. In the inset dots and continuous line show the experimental and simulated patterns, respectively. Vertical bars show the position of

the Bragg's reflections and the continuous bottom line is the difference among the experimental and simulated patterns. It was found that NBMO-30 crystallizes into the body-centered orthorhombic crystal structure and all the reflections in the XRD profiles can be indexed by *Imma* space group. The unit cell lattice parameters (a, b, c, and V) increase with the increasing particle size of the NBMO-30 manganite.

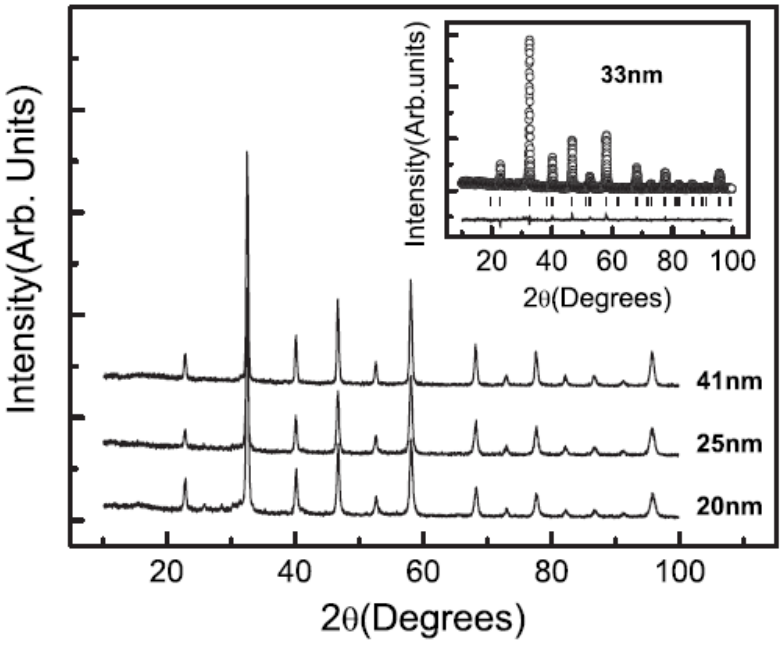

Figure 1.14: RT powder XRD patterns of NBMO-30 NPs having particle size 20, 25 and 41 nm. The inset shows the Rietveld fit of XRD data of the sample having particle size 33 nm [after Roy et al. (2008)].

Fig. 1.15 demonstrates temperature dependence of zero field cooled (ZFC), and field cooled (FC) magnetizations for NBMO-30 NPs measured under a magnetic field of 100 Oe after Roy et al. (2008). The FC and ZFC magnetizations display an extensive deviation at low temperatures, and a hump is detected in the ZFC magnetization plot. All the samples of NBMO-30 manganite exhibit PM to FM transition. Inset of **Fig. 1.15** shows dM/dT vs. T curves for the determination of the value of Curie-temperature (T_C)

corresponding to the minimal peak in the curves, which increases with the increasing particle size of the NBMO-30 manganite.

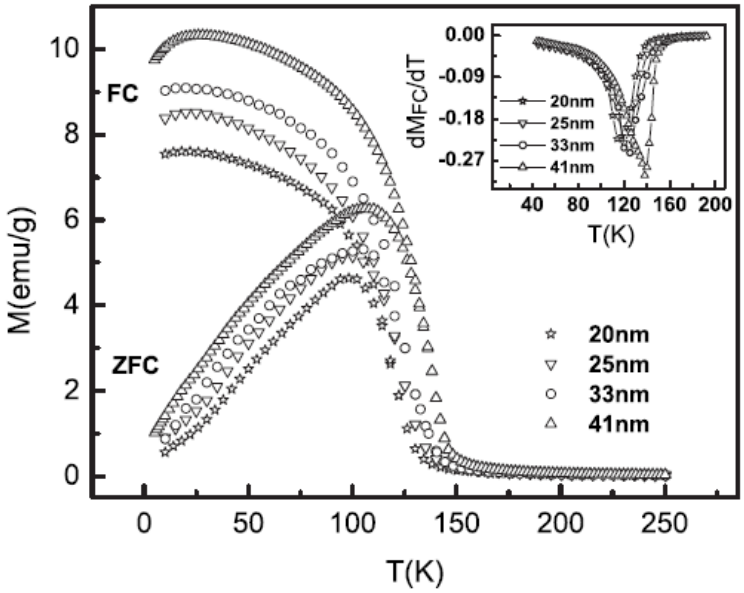

Figure 1.15: The temperature dependence of ZFC and FC dc magnetizations of NBMO-30 NPs. The inset shows plots between dM/dT and T [after Roy et al. (2008)].

Roy et al. (2008) also reported the magnetic field dependent dc magnetization hysteresis for NBMO-30. **Fig. 1.16** demonstrates magnetization (M) vs. magnetic field (H) plots measured at different temperatures in the range 25 to 250 K for NBMO-30 manganite having particle size 20 nm. The M(H) curves at low temperature clearly display hysteresis loop like ferromagnets with leading Curie-like part, but as temperature increases, the thickness of the hysteresis loop reduces quickly, and finally, the behavior of the M(H) curves turns into linear at high temperatures representing PM behavior. The top inset of **Fig. 1.16** presents the virgin branch of the M(H) plots, which do not reach at saturation value even up to the magnetic field of 5 T. This non-attainment of saturation of the magnetization is more obvious in the M(H) plot measured at 5 K, as shown in the bottom inset of **Fig. 1.16**.

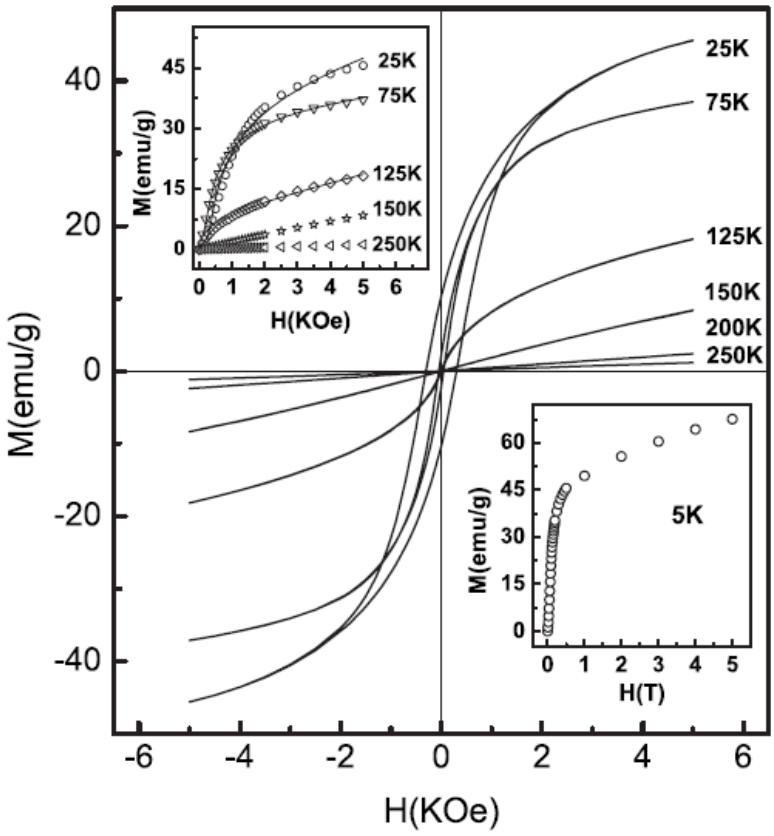

Figure 1.16: Field dependent magnetization of NBMO-30 NPs with 20 nm size measured at various temperatures (25 K ≤ T ≤ 250 K). Top inset displays the virgin M(H) plots, and the bottom inset shows the unsaturation of magnetization at 5 K [after Roy et al. (2008)].

Fig. 1.17 demonstrates temperature-dependent variation in the ac susceptibility for the NBMO-30 sample with particle size 20 nm measured at various frequencies. In this figure (a) shows the real part $\chi'(T)$ of the ac susceptibility and (b) presents the imaginary part $\chi''(T)$ of the ac susceptibility. The in-phase component of the ac susceptibility displays a broad peak near to T_B, which does not depend on the frequency. The out-phase component of ac susceptibility also displays a frequency independent major peak near to T_{irr} simultaneously having a peak at the lower temperature. The equivalent characteristic is not present in $\chi'(T)$, and this may occur as a result of the large $\chi'(T)$ coupled with ferromagnetism. At low temperature, the peaks

in $\chi''(T)$ are frequency dependent (T_f) and shifted towards higher temperature side with increasing frequency. They performed its qualitative as well as quantitative analysis using various models and found that the NPs of NBMO-30 exhibit a glasslike cluster behavior.

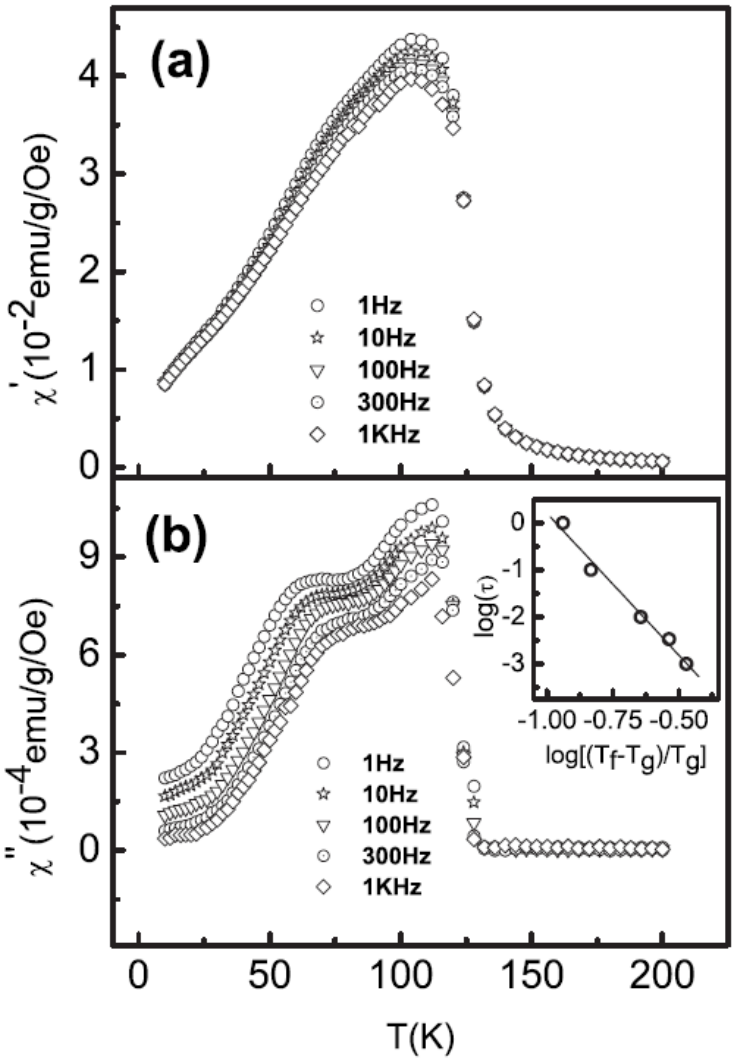

Figure 1.17: Temperature dependent (a) real $\chi'(T)$ and (b) imaginary part $\chi''(T)$ of ac-susceptibility for NBMO-30 sample with a particle size of 20 nm measured at 4 Oe ac field for different frequencies. The inset of (b) demonstrates the $\log(\tau)$ vs. $\log[(T_f - T_g)/T_g]$ plot with the best linear fit [after Roy et al. (2008)].

Roy et al. (2008) also presented magneto-resistive behavior of NPs of NBMO-30 manganite. They observed that the magnitude of the MR in the region of low field increases quickly, whereas, in the region of high field MR changes gradually with increasing intensity of magnetic field and decreases with increasing temperature and exhibit maximum MR of ~90% at 20 K. They suggested that this magnetic field dependent variation in MR can be explained by invoking a model considering the role of spin-polarized tunneling at the grain boundaries, and this model was effectively applied in case of polycrystalline substances in addition to thin films. **Figs. 1.18**(a-b) display magnetic field dependent MR for NBMO-30 manganite having particle size 20 and 25 nm, respectively.

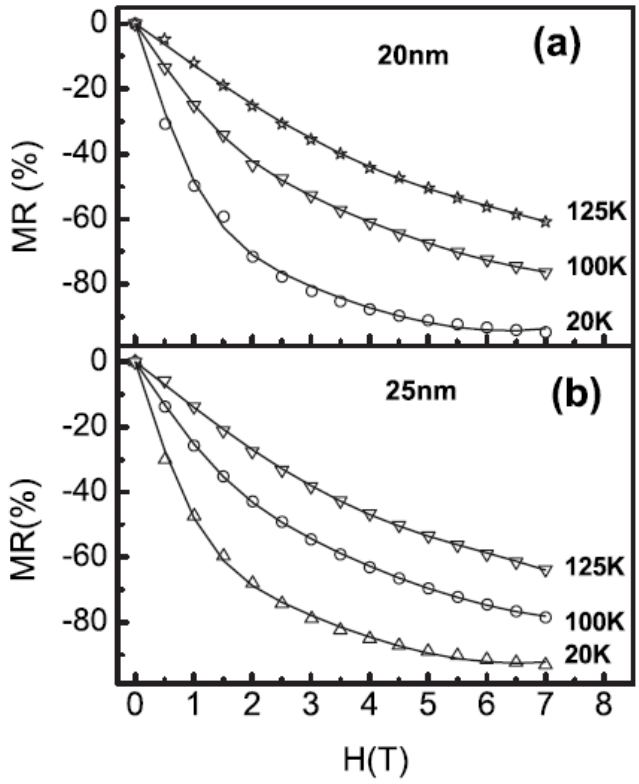

Figure 1.18: Magnetic field dependent variation in MR for NPs of NBMO-30 with the particle size (a) 20 nm and (b) 25 nm measured at different temperatures [after Roy et al. (2008)].

1.9.2. Structural and Magnetic Phase Diagrams for $La_{1-x}Ba_xMnO_3$ Manganites

Ju et al. (2000) studied the structural and magnetic behaviors of $La_{1-x}Ba_xMnO_3$ (LBMO) manganites for the composition range $0 \leq x \leq 1$. They presented structural and magnetic phase diagrams for LBMO manganite. **Fig. 1.19** shows the structural phase diagram (variation in unit cell parameters) for LBMO. It has been reported by Ju et al. (2000) that LBMO exhibits tetragonal structure for $0 < x \leq 0.13$, rhombohedral structure for $0.13 < x \leq 0.38$, cubic structure for $0.38 < x \leq 0.5$ and cubic and an unidentified phase for $x > 0.5$ (see **Figs. 1.19 & 1.21**). The unit cell lattice parameters increase with enhancing concentration of Ba^{2+}-ion at La-site due to larger ionic size of Ba^{2+}-ion (r_{Ba}^{2+} = 1.61 Å and r_{La}^{3+} = 1.36 Å) [Ju et al. (2000)].

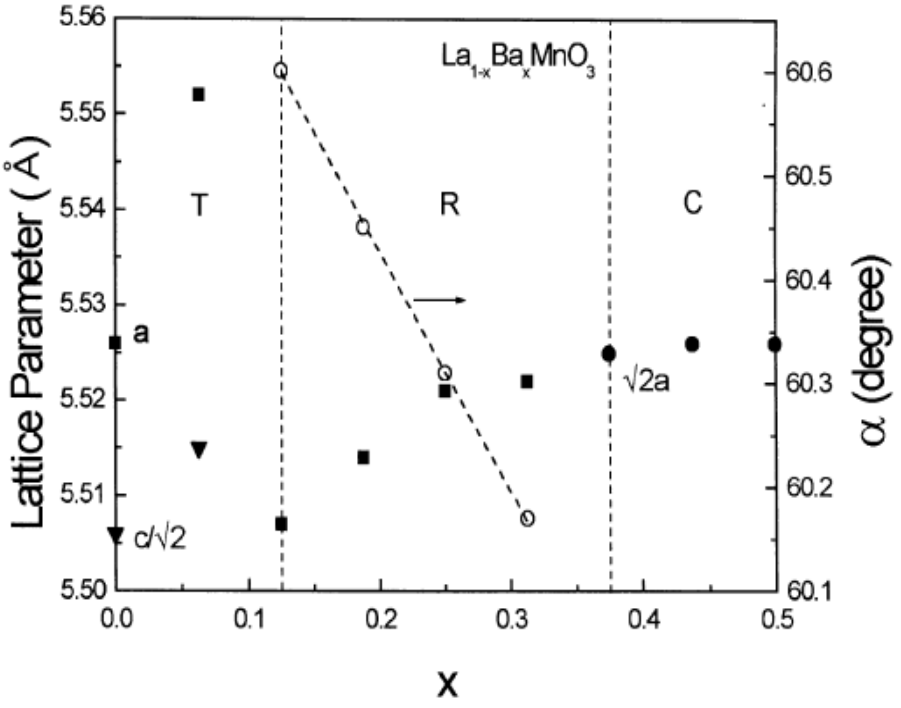

Figure 1.19: Unit-cell parameters of $La_{1-x}Ba_xMnO_3$ for $0 \leq x \leq 0.5$ [T = tetragonal, R = rhombohedral, C = cubic] (after Ju et al. (2000)).

The magnetic phase diagram for LBMO manganite is shown in **Fig. 1.20** as reported by Ju et al. (2000). They found that LBMO manganite displays FM insulator with single domain spin clusters for $x < 0.2$, fully FM metallic for $0.2 < x < 0.5$ and FM multiphase for $x \geq 0.5$ with multi-domain FM particles implanted in a non-FM medium below the critical temperature, however, above critical temperature it exhibits PM insulator behavior. The values of T_C increase quickly with increasing Ba-concentration up to $x = 0.3$, and after that, the values of T_C remain almost constant. For $x \geq 0.3$, LBMO shows T_C well above room temperature.

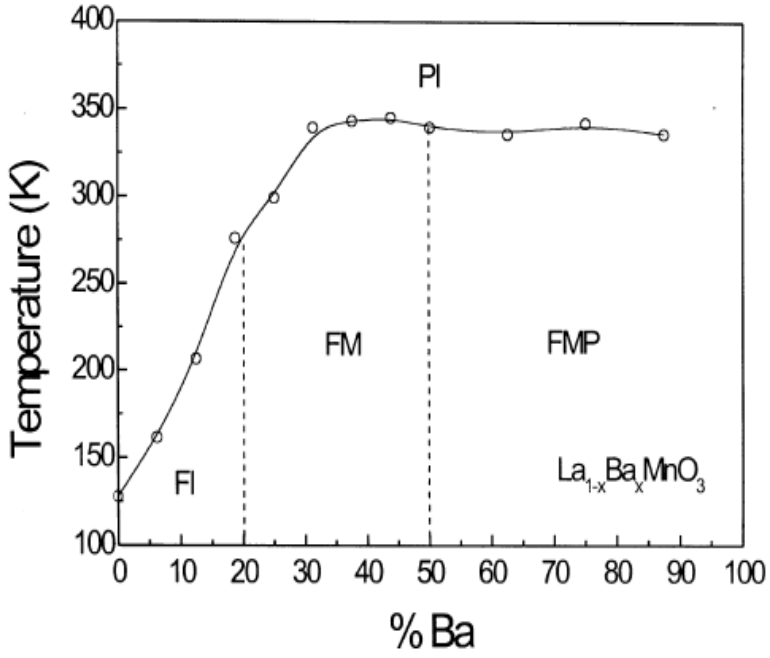

Figure 1.20: The magnetic phase diagram of LBMO as a function of Ba^{2+}-ion doping concentration (x) and temperature (T) [FI = FM insulator, FM = FM metal, and FMP = FM multiphase (after Ju et al. (2000))].

The beauty of $La_{1-x}Ba_xMnO_3$ system is that it displays FM behavior in the entire range of the compositions. **Fig. 1.21** shows variation of saturation magnetization with doping concentration of Ba^{2+}-ion (x) measured at 5 K. The value of saturation magnetization first increases for $0 \leq x \leq 0.13$ and then decreases slowly for $0.13 < x \leq$

0.5, however, above x > 0.5 (cubic + unidentified phases), it decreases rapidly and has value less than theoretical value with enhancing concentration of Ba^{2+}-ion.

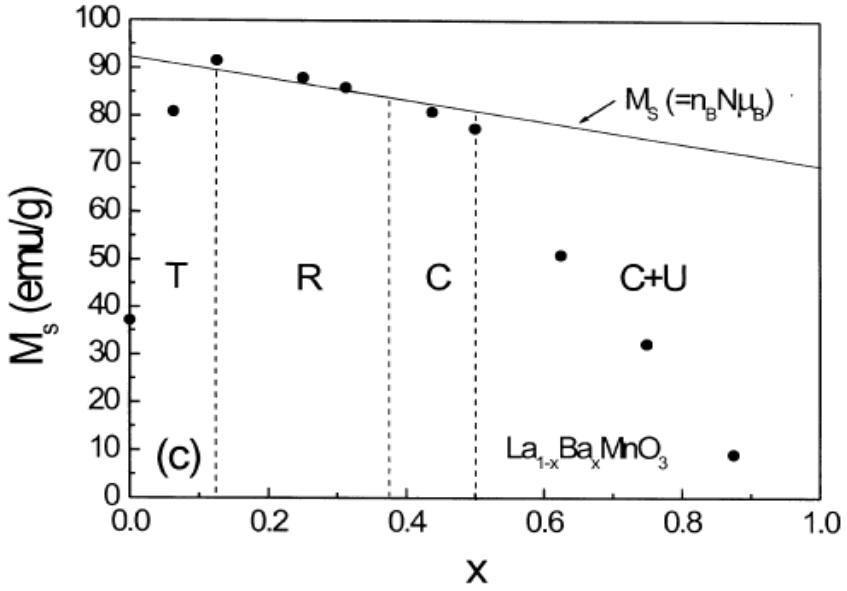

Figure 1.21: The doping concentration dependence of the saturation magnetization M_s for LBMO obtained at T = 5 K. T = tetragonal, R = rhombohedral, C = cubic and U = unidentified phase [after Ju et al. (2000)].

1.9.2.1. Structural and Magnetic Properties of $La_{0.6}Ba_{0.4}MnO_3$ Manganite

The 40 mol% Barium doped $LaMnO_3$ (LBMO-40) perovskite has not been studied so far in details. There are very few literature available on LBMO-40 manganite. Different research groups have a different opinion on the crystal structure of LBMO-40. According to Ju et al. (2000) and Barnabe et al. (1998), the crystal structure of LBMO-40 has the cubic structure with $Pm\bar{3}m$ space group; while it has a rhombohedral structure with $R\bar{3}m$ space group according to Hussain et al. (2016) and McBride et al. (2017). However, all research groups have reported that LBMO-40 manganite exhibits long-range ferromagnetic ordering around 335 K. Hussain et al. (2016) studied magnetocaloric effect in LBMO-40 manganite in terms of magnetic

entropy change with magnetic field and found maximum entropy change of ΔS_M =1.192 J/kg.K and relative cooling power (RCP) of 79.31 J/kg for 2.5 T field. This shows that LBMO-40 manganite can be considered as an active magnetic refrigerant near room temperature. **Fig. 1.22** shows temperature-dependent variation in change in entropy at various magnetic field and change in RCP with the applied magnetic field which increases linearly for LBMO-40 manganite.

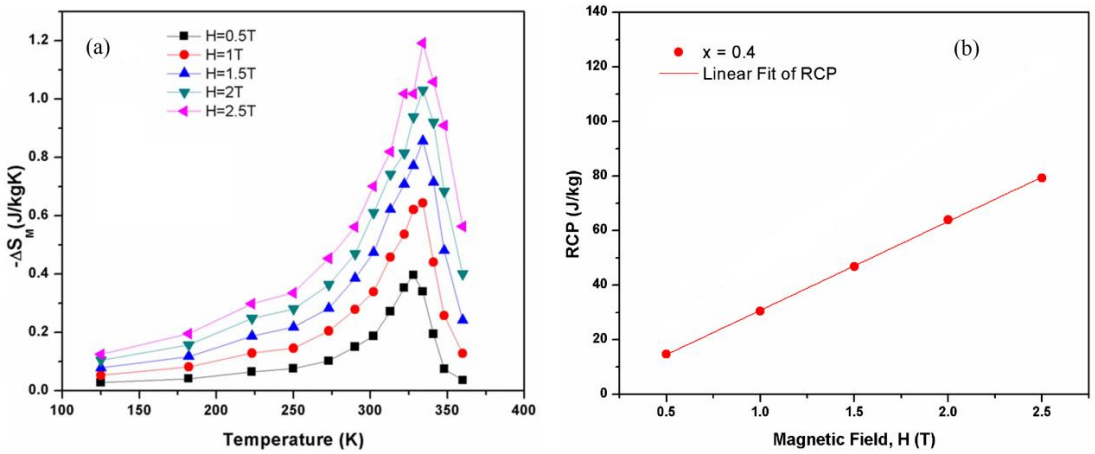

Figure 1.22: (a) Magnetic entropy change as a function of temperature and (b) the RCP values as a function of applied magnetic field for LBMO-40 manganite [after Hussain et al. (2016)].

1.9.3. Effect of doping of Magnetic/Non-magnetic ions at Mn-site in Perovskite Manganites

In the recent years, several studies has been carried out, for the effect of Mn-site doping in perovskite manganites, on the structural, magnetic, magnetocaloric, transport, optical and electrical behaviors because they result in exciting phenomena and properties [Abdouli et al. (2019); Dang et al. (2018); Troyanchuk et al. (2017); Ho et al. (2016); Zhu et al. (2006); Dho et al. (2002); Gayathri et al. (1997)]. Abdouli et al. (2019) studied the effect of doping of Fe^{3+}-ions (magnetic) at Mn-site on structural,

magnetic and magnetocaloric properties for $La_{0.5}Sm_{0.2}Sr_{0.3}Mn_{1-x}Fe_xO_3$ (LSSMFO) manganites with $0 \leq x \leq 0.15$ synthesized using auto-combustion method. They found that LSSMFO crystallizes into orthorhombic crystal structure with the *Pnma* space group, in which unit cell volume increases with increasing concentration of Fe^{3+}-ions. The LSSMFO manganites undergo second-order PM to FM phase transition at T_C which decreases with increasing concentration of Fe^{3+}-ions due to the reduction of DE interaction between Mn^{3+} and Mn^{4+} through O^{2-}. The analysis of the magnetocaloric effect in LSSMFO manganites reveals a maximum magnetic entropy change near T_C under a magnetic field change of 5 T of 3.06, 2.93, 2.22 and 0.77 $J.kg^{-1}.K^{-1}$, and display high RCP values of 268, 280, 285 and 226 $J.Kg^{-1}$ for x = 0, 0.05, 0.10 and 0.15, respectively. These values are adequate enough for prospective application in magnetic refrigeration near RT.

1.9.3.1. Impact of Ti-doping on Structural, Magnetic and Transport Properties of $La_{0.7}Sr_{0.3}Mn_{1-x}Ti_xO_3$ ($0 \leq x \leq 0.5$) Thin Films

Zhu et al. (2006) studied the effect of Ti^{4+}-ions (non-magnetic) substitution at Mn-site on the crystal structure, magnetic and transport properties of $La_{0.7}Sr_{0.3}Mn_{1-x}Ti_xO_3$ (LSMTO) thin films with $0 \leq x \leq 0.5$ deposited by using chemical solution deposition (CSD) technique. **Fig. 1.23** shows room temperature XRD patterns of LSMTO films. It was found that all the XRD patterns can be indexed by pseudocubic structure; furthermore, it is noticeable that all the films are extremely (h00)-oriented. The inset (a) of **Fig. 1.23** shows that the diffraction peaks in the XRD patterns for $x \leq 0.3$ shifted towards lower angle side with increasing concentration of Ti^{4+} indicating expansion in lattice constant, however, for $x > 0.3$, diffraction peaks shifted towards higher angle side showing reduction in the lattice constant as shown in the inset of (b). Variation in lattice constant can be explained by using the concept of ionic radii. For $x \leq$

0.3 the lattice enlargement with the increase in Ti^{4+} concentration results from the substitution of the smaller Mn^{4+} ion (r = 0.53 Å) by the comparatively larger ionic Ti^{4+} (r = 0.605 Å). Since the concentration of Mn^{4+} ions in $La_{0.7}Sr_{0.3}MnO_3$ (LSMO) manganite is about 0.3, hence, for x > 0.3, Ti^{4+} has to replace some Mn^{3+} having a larger ionic radius (r = 0.645 Å).

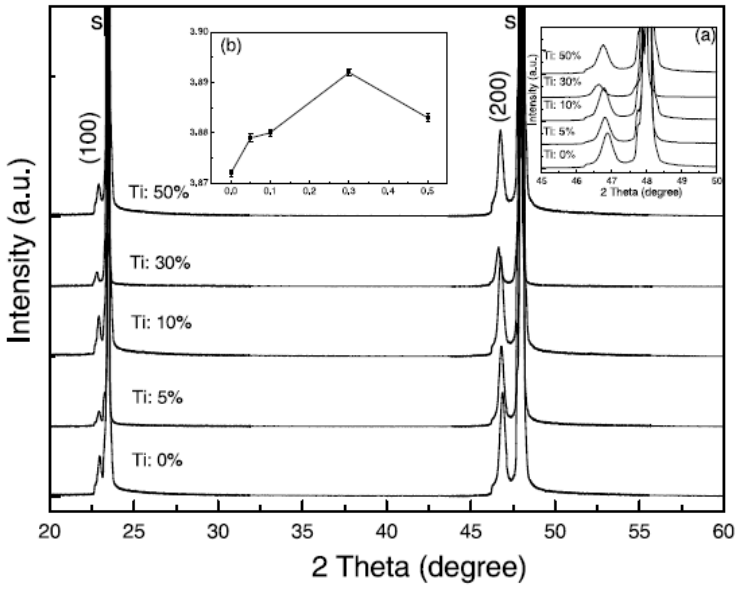

Figure 1.23: RT XRD patterns for the LSMTO ($0 \leq x \leq 0.5$) thin films on $LaAlO_3$ (LAO) substrates. The Bragg's peaks indicated by letter "s" correspond to the substrates. Inset (a) displays the zoomed XRD patterns between $2\theta = 45°$-$50°$ of the films, and the inset (b) indicates variation in lattice constant vs. Ti^{4+} content [after Zhu et al. (2006)].

Fig. 1.24 demonstrates the magnetic field dependent magnetization M(H) for all LSMTO films at RT. It can be clearly seen that the saturation magnetization (M_s) decreases with increasing the concentration of Ti^{4+} due to the weakening of DE interaction. Nevertheless, it is exciting to find that all samples have clear M(H) loops at RT, which point outs that in the CSD-derived Ti^{4+} substituted LSMO films, it is simple

to maintain the weak FM behavior even when the concentration of Ti^{4+} is high, and this may be connected to the extensively-studied phase separation phenomenon.

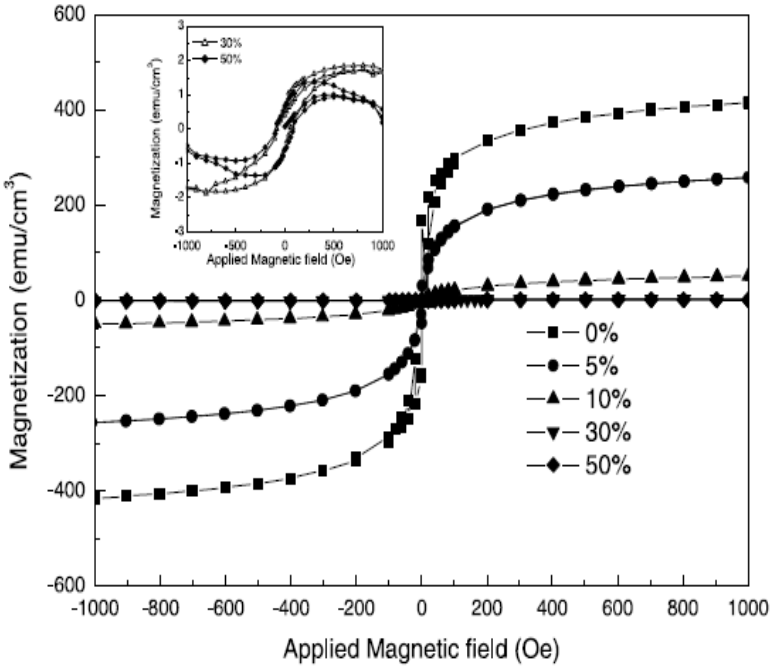

Figure 1.24: The magnetic field dependent magnetic hysteresis of LSMTO films at room temperature [after Zhu et al. (2006)].

Zhu et al. (2006) also studied the magnetic field and temperature dependence of MR of the LSMTO samples with $x \leq 0.3$. **Fig. 1.25** shows the variation in MR as a function of temperature for LSMTO manganites with $x \leq 0.3$. One can clearly see that the temperature corresponding to the maximum MR shifted towards the lower side. However, maximum MR value constantly increases, and the characteristic transition gets broaden with enhancing the concentration of Ti^{4+}-ions, which is a very useful characteristic for potential applications.

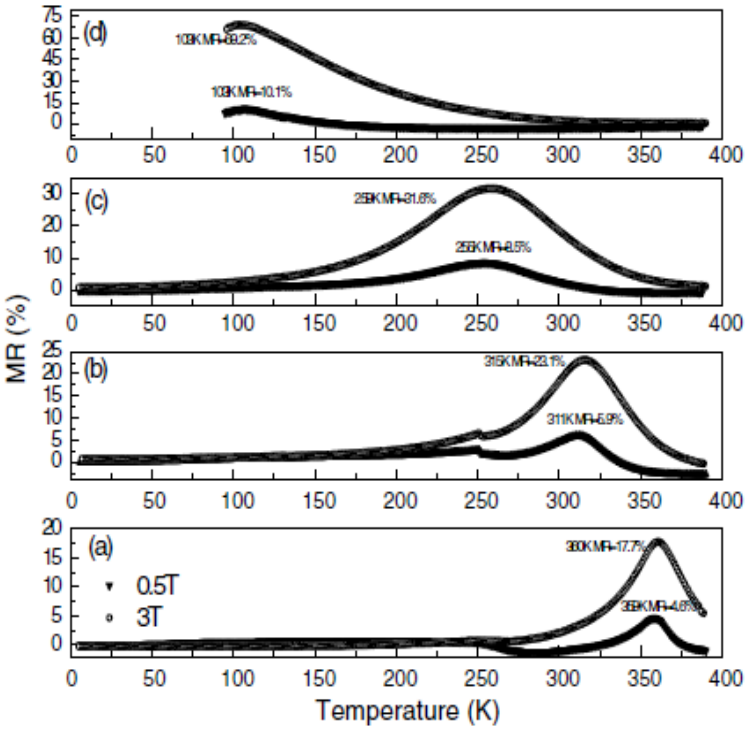

Figure 1.25: Temperature dependence of MR at different fields (0.5 T and 3 T) of LSMTO films for (a) x = 0, (b) x = 0.05, (c) x = 0.1 and (d) x = 0.3 [after Zhu et al. (2006)].

1.9.3.2. Effect of Ti-doping at Mn-site on Structural and Magnetic Properties of $La_{0.67}Ba_{0.33}Mn_{1-x}Ti_xO_3$ ($0 \leq x \leq 0.3$) Manganites

Gasmi et al. (2009) investigated the influence of Ti^{4+} ion substitution on structural and magnetic behaviors of $La_{0.67}Ba_{0.33}Mn_{1-x}Ti_xO_3$ (LBMTO) manganites with $0 \leq x \leq 0.3$. They studied the effect of doping of Ti^{4+} ion on the crystal structure by performing Rietveld structure refinement using XRD and neutron diffraction patterns and found that all samples crystallize into the rhombohedral structure with $R\bar{3}c$ centrosymmetric space group. The values of lattice constants and average bond length <(Mn,Ti)-O> increase with the enhanced doping concentration of Ti^{4+}-ions due to the replacement of Mn^{4+} (r = 0.53 Å) cation by Ti^{4+} (r = 0.605 Å) cation as depicted in **Fig. 1.26**.

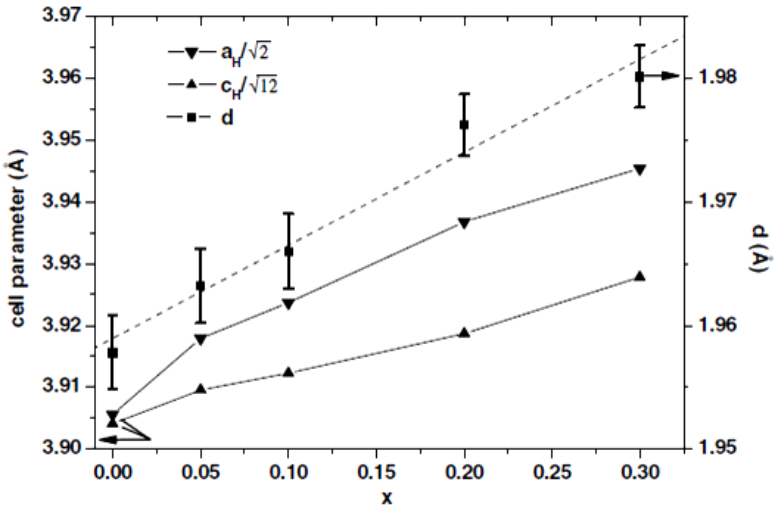

Figure 1.26: Structural parameters (lattice parameters and average bond length between Mn/Ti-O) acquired from the Rietveld analysis of the XRD profiles as a function of the doping concentration of Ti^{4+}-ion (x) for $La_{0.67}Ba_{0.33}Mn_{1-x}Ti_xO_3$ ($0 \leq x \leq 0.3$) manganites [after Gasmi et al. (2009)].

Fig. 1.27 shows temperature-dependent variation in magnetizations collected in ZFC mode at an applied field of 500 Oe for LBMTO manganites. The temperature dependent magnetization curves reveal that all Ti-doped samples go through PM to FM phase transition at T_C. The value of T_C reduces drastically from 332 K for x = 0 to 20 K for x = 0.3 with increasing doping concentration of Ti^{4+}-ion. The reduction in the T_C can be explained on the basis of reduction in the DE interaction among Mn^{4+} and Mn^{3+} cations.

Gasmi et al. (2009) recorded magnetic field dependent magnetization M(H) at 50 K up to 100 kOe for LBMTO manganites as displayed in **Fig. 1.28**. The M(H) curve for parent sample (x = 0) gets completely saturated at higher magnetic field, exhibiting long-range FM ordering. With increasing Ti content, saturation of the M(H) plots decreases slowly for low doped samples and rapidly for highly doped samples. The behavior of unsaturation of magnetization confirms the existence of short-range AFM

ordering with predominating FM state. The fraction of the AFM ordering increases with enhancing doping concentration of Ti^{4+}-ion.

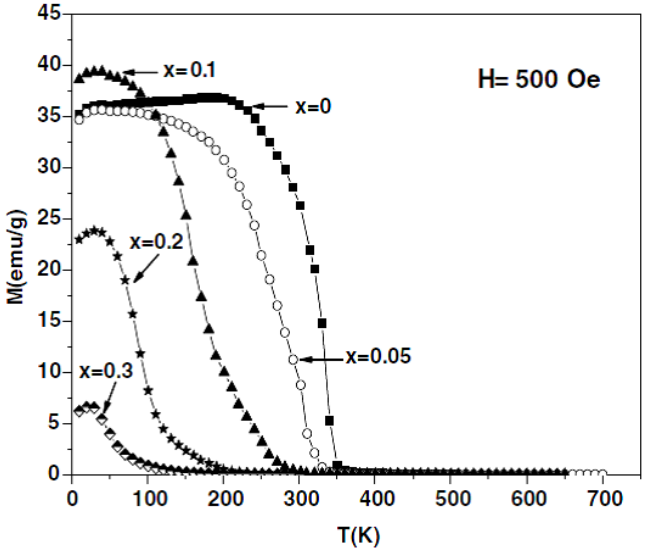

Figure 1.27: Compositions dependence of the magnetization recorded at a constant magnetic field H = 500 Oe as a function of temperature for $La_{0.67}Ba_{0.33}Mn_{1-x}Ti_xO_3$ ($0 \leq x \leq 0.3$) perovskites [after Gasmi et al. (2009)].

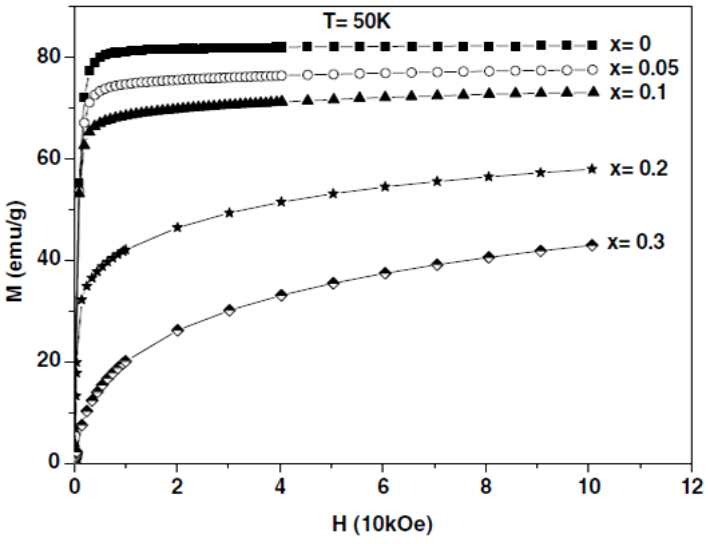

Figure 1.28: Magnetic field dependence of magnetization measured at 50 K for for $La_{0.67}Ba_{0.33}Mn_{1-x}Ti_xO_3$ ($0 \leq x \leq 0.3$) manganites [after Gasmi et al. (2009)].

1.9.3.3. Effect of Ti-doping on the Critical Behavior, Magnetic and Magnetocaloric Properties in Disordered Ferromagnets $La_{0.7}Ba_{0.3}Mn_{1-x}Ti_xO_3$ (x = 0.05 and 0.1)

Ho et al. (2016) investigated effect of doping of Ti^{4+} cation on magnetic and magnetocaloric properties. Based on the Franco's universal curves and Banerjee's criteria, they showed that $La_{0.7}Ba_{0.3}Mn_{1-x}Ti_xO_3$ manganites display a PM to FM second-order magnetic transition. They estimated critical parameters using modified Arrott's plot method and found T_C = 245 K, β = 0.374(13), γ = 1.228(45), and δ = 4.26(3) for x = 0.05, and T_C = 169 K, β = 0.339(1), γ = 1.307(3), and δ = 4.78(2) for x = 0.1, where β, γ and δ are critical exponents of the order parameters for various models. The calculated values of β = 0.374 for x = 0.05 and 0.339 for x = 0.1 suggests that the nature of the magnetic interactions of the studied samples falls into the 3D Heisenberg (β = 0.365) and 3D Ising model (β = 0.325), respectively, analogous to short-range FM ordering due to FM clusters in a broad temperature range even above T_C [Kaul (1985)]. Study of magnetocaloric effect near T_C shows a maximum change in magnetic entropy ($|\Delta S_{max}|$) of about 4 and 3 $Jkg^{-1}K^{-1}$ for a magnetic field change 5 T, which correspond to the RCP values of ~190 and 240 J/kg for x = 0.05 and 0.1, respectively. **Fig. 1.29** displays temperature dependent variation of saturation magnetization $M_S(T)$ and inverse initial magnetic susceptibility $\chi_0^{-1}(T)$ for $La_{0.7}Ba_{0.3}Mn_{1-x}Ti_xO_3$ with x = 0.05 and 0.1 manganites.

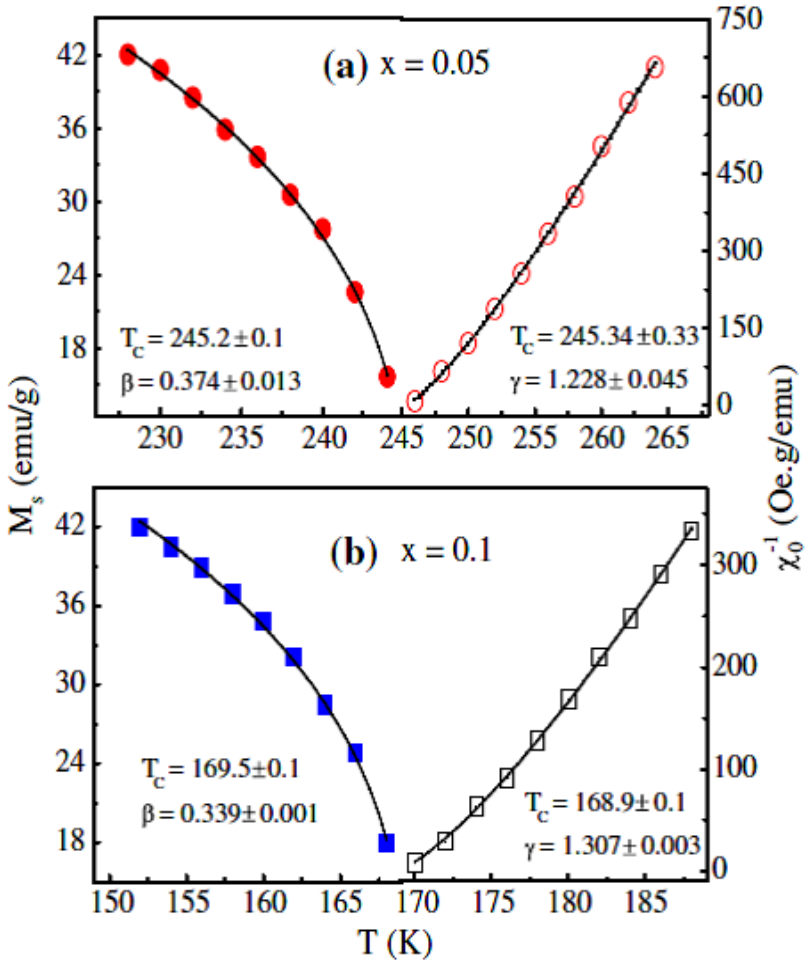

Figure 1.29: Temperature dependent of $M_S(T)$ and $\chi_0^{-1}(T)$ data for $La_{0.7}Ba_{0.3}Mn_{1-x}Ti_xO_3$ manganites with (a) x = 0.05, (b) x = 0.1 [after Ho et al. (2016)].

1.9.3.4. Effect of Cr-doping at Mn-site on Magnetic Behaviors in $La_{0.46}Sr_{0.54}Mn_{1-x}Cr_xO_3$ ($0 \leq x \leq 0.08$) Manganites

Dho et al. (2002) explored consequences of Cr-doping on magnetic behaviors of $La_{0.46}Sr_{0.54}Mn_{1-x}Cr_xO_3$ (LSMCO) ($0 \leq x \leq 0.08$) perovskites. **Fig. 1.30** shows magnetizations as a function of temperature recorded in ZFC and FC conditions and measured at a constant field of 50 Gauss (G). All the samples show PM to FM magnetic transition near RT at T_C. The parent sample with x = 0 shows two sharp magnetic transitions; PM to FM at 272 K and FM to AFM around 190 K. With increase in Cr-doping concentration, the extent of AFM phase fraction decreases and completely

vanishes for x = 0.08. This undoubtedly reveals that the impurity of Cr^{3+} ions alters the magnetic ground state from AFM to FM. This can be attributed to the enhancement of the FM-DE interaction among Cr^{3+} and Mn^{3+} ions through O^{2-} anion. In the FM state, a large difference within the FC and ZFC magnetization plots is attributed to the pinning of the domain wall. Nevertheless, their magnetic properties are entirely different for the LSMCO samples having low Cr-doping concentration. Additionally, the LSMCO sample with x = 0.02 displays spin-glass (SG) like behavior in low temperature around 40 K, which is confirmed by a cusp in the ZFC magnetization and a characteristic difference between the FC and ZFC magnetization curves.

The temperature dependent real $\chi'(T)$ and imaginary parts $\chi''(T)$ of ac magnetic susceptibility for the LSMCO sample with x = 0.02 at different frequencies reported by Dho et al. (2002) are shown in **Fig. 1.31(a)**. All the measurements were recorded at a constant ac magnetic field of 10 G in ZFC condition upon cooling from RT. The $\chi'(T)$ and $\chi''(T)$ susceptibility plots show sudden upturns about 280 K, showing a PM to the FM phase transition. A quick fall in both the $\chi'(T)$ and $\chi''(T)$ plots around 170 K is associated with a transition from FM to AFM. With further reducing the temperature below 170 K, the $\chi'(T)$ and $\chi''(T)$ curves show a cusp around 40 K and 35 K, respectively, which shifted towards higher temperature side when the measurement frequency is increased. These characteristics are indicative of frustration of the long-range AFM phase, which is usually known as reentrant spin-glass (RSG) state. The RSG systems are that in which SG re-renters into a long-range magnetically ordered state below SG transition (T_{SG}). With reducing temperature the well known RSG systems experience a successional magnetic transition of either PM to AFM to RSG or PM to FM to RSG.

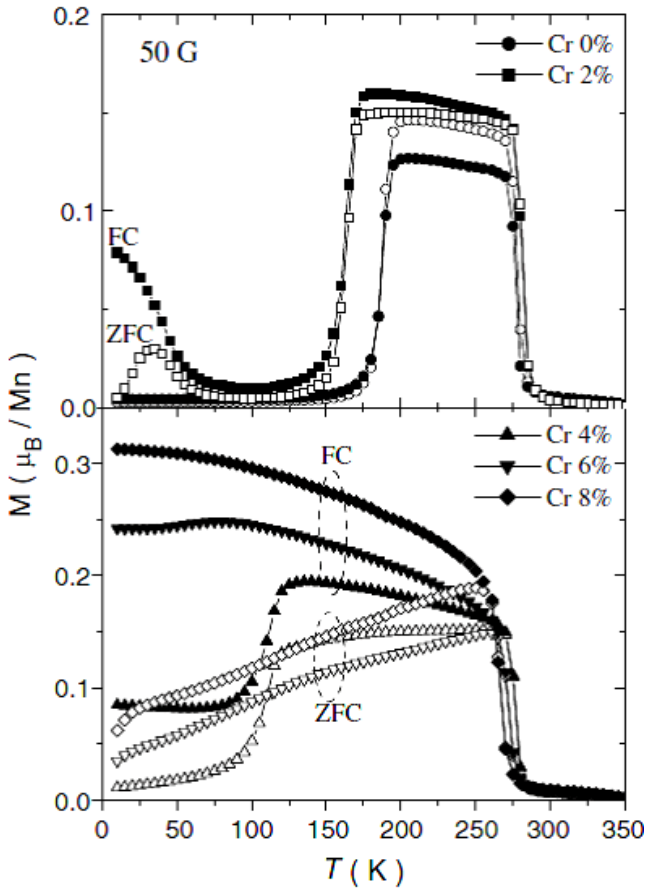

Figure 1.30: Temperature dependent magnetization for $La_{0.46}Sr_{0.54}Mn_{1-x}Cr_xO_3$ ($0 \leq x \leq 0.08$) manganites measured at H = 50 Gauss under ZFC and FC conditions [after Dho et al. (2002)].

Conventional critical slowing down model quantifies the shift in the freezing temperature (T_f) corresponding to the maxima peak at low temperatures given by Equation (1.6):

$$\frac{\tau}{\tau_0} = \left[\frac{T_f - T_{SG}}{T_{SG}}\right]^{-z\upsilon} \tag{1.6}$$

Where τ is relaxation time, τ_0 is characteristic relaxation time having a typical value of 10^{-10}-10^{-13} s for spin-glass systems, and $z\upsilon$ is critical exponent having value 4-13 for conventional spin-glasses [Luo et al. (2015)]. The inset of **Fig. 1.26**(a) displays the excellent fits using above equation to the data in the frequency range 10-10000 Hz, representing that the SG state can be well illustrated by the slowing down model, which

provides the values of zυ and T_{SG} for χ'(T) as 7.6 and 40.8 K, respectively, and for χ"(T) T_{SG} = 34.1 K and zυ = 10.7. This suggests that LSMCO manganites with x = 0.02 exhibits conventional spin-glass behavior of reentrant type.

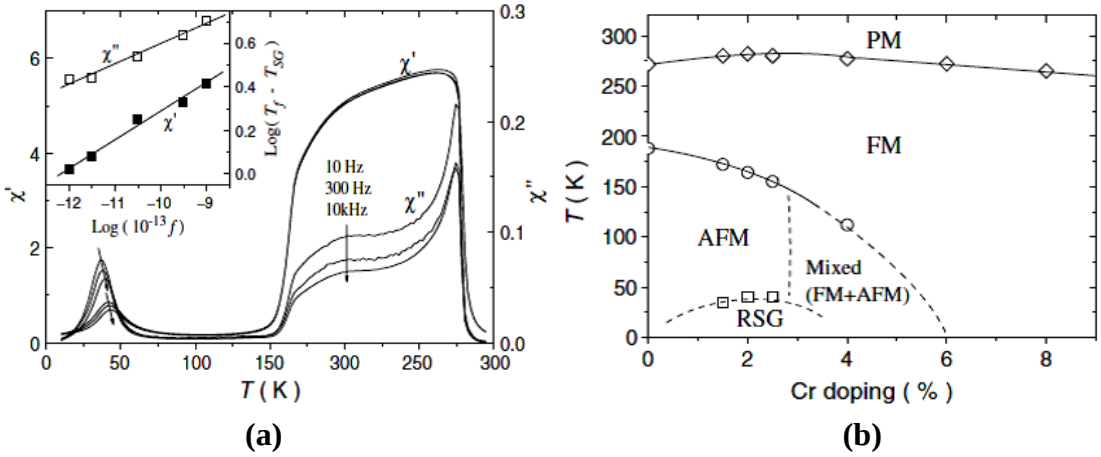

(a) **(b)**

Figure 1.31: (a) The temperature dependent variation of the ac magnetic susceptibility recorded at various frequencies for $La_{0.46}Sr_{0.54}Mn_{0.98}Cr_{0.02}O_3$ manganite collected at H_{ac} = 10 G. The inset displays the best linear fits of the χ'(T) and χ"(T) data. (b) Magnetic phase diagram between temperature and Cr-doping concentration (x) for $La_{0.46}Sr_{0.54}Mn_{1-x}Cr_xO_3$ manganites [after Dho et al. (2002)].

On the basis of the magnetic data studied, Dho et al. (2002) constructed a comprehensive magnetic phase diagram for the Cr-doped $La_{0.46}Sr_{0.54}Mn_{1-y}Cr_yO_3$ ($0 \leq x \leq 0.08$) compounds as shown in **Fig. 1.31(b)**. In this magnetic phase diagram, there is a noticeable RSG state that lies in the region of low Cr-doping concentration in $La_{0.46}Sr_{0.54}Mn_{1-x}Cr_xO_3$ manganites. With decreasing temperature, the Cr-doped system undergoes various phase transitions from PM to RSG through FM and AFM phases. When the content of the Cr^{3+} ion enhances, the FM phase slowly overcomes the AFM ground state.

1.9.3.5. Impact of Cobalt doping on Structural, Magnetic and Magnetotransport Properties of $La_{0.7}Sr_{0.3}Mn_{1-x}Co_xO_3$ ($0.13 \leq x \leq 1$) Perovskites

Troyanchuk et al. (2017) studied impact of cobalt doping on crystal structure, magnetic and magnetotransport behaviors of $La_{0.7}Sr_{0.3}Mn_{1-x}Co_xO_3$ ($0.13 \leq x \leq 1$) perovskites. They studied structural behavior using XRD and neutron diffraction data and found that all the samples crystallize into rhombohedral structural with $R\bar{3}c$ space group both at 300 K and 2 K. The values of unit cell volume decreases with enhancing concentration of Co^{3+}-ion as its radius is less than the radius of Mn^{3+}-ion. The temperature dependence of magnetization analysis reveals that all the samples exhibit PM to FM transition, however, T_C decreases from 270 K for x = 0.13 to 140 K for x = 0.33 and increases to 190 K for x = 0.5, decreases to 68 K for x = 0.8 and further increases to 225 K for x = 1 ($La_{0.7}Sr_{0.3}CoO_3$) with increasing concentration of Co^{3+}-ion as shown in **Fig. 1.32**.

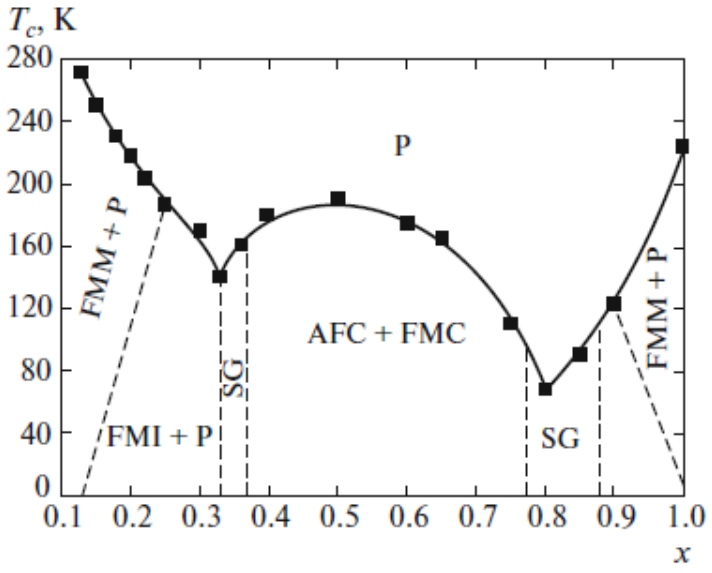

Figure 1.32: Magnetic phase diagram for $La_{0.7}Sr_{0.3}Mn_{1-x}Co_xO_3$ perovskites, where, P = PM phase; FMM = metallic FM phase; FMI = insulating FM phase; AFC + FMC = ion-ordered phase consisting of AFM and FM clusters; and SG = spin glass [after Troyanchuk et al. (2017)].

Fig. 1.32 shows magnetic phase diagram for $La_{0.7}Sr_{0.3}Mn_{1-x}Co_xO_3$ perovskites, which clearly indicates various magnetic states in different composition and temperature regions. To further explore the magnetic property, Troyanchuk et al. (2017) performed field dependent magnetization measurements. **Fig.1.33** displays magnetic field dependence of magnetization M(H) curves of $La_{0.7}Sr_{0.3}Mn_{1-x}Co_xO_3$ for x = 0.13, 0.3, 0.33, 0.4, 0.5, 0.65, 0.85 and 1 measured at 10 K. The M(H) curves show that magnetization decreases with increasing concentration of Co^{3+}-ion for x = 0.13 to 0.65 and increases with further increasing concentration of Co^{3+}-ion for x = 0.65 to x = 1.

Troyanchuk et al. (2017) also studied magnetoresistive behavior of $La_{0.7}Sr_{0.3}Mn_{1-x}Co_xO_3$ perovskites and found that in the composition range $0.3 \leq x \leq 0.4$, magneto-resistive effect (MR) reaches 97 % and decreases slowly with rising temperature without any anomalies near T_C. At $x \leq 0.2$, the MR increases close to T_C.

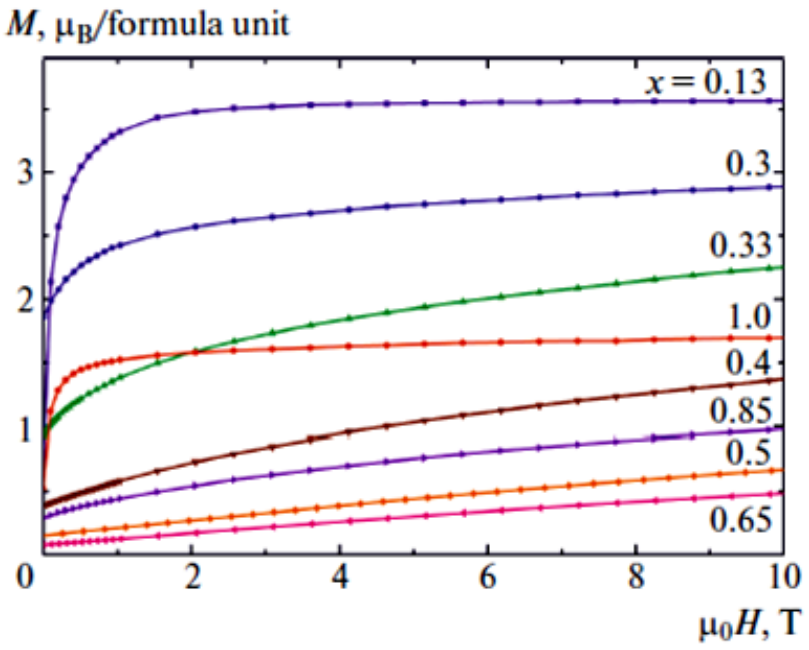

Figure 1.33: Field dependence of the magnetization for $La_{0.7}Sr_{0.3}Mn_{1-x}Co_xO_3$ perovskites at T = 10 K [after Troyanchuk et al. (2017)].

1.10. Motivations behind the Present Work

For the present thesis work, we have selected to parent compounds $Nd_{0.7}Ba_{0.3}MnO_3$ and $La_{0.6}Ba_{0.4}MnO_3$ for which we planned to investigate the effect of Ti-substitution at Mn-site. As discussed in the earlier sections, these systems are less explored and to the best of our knowledge, there is no report on the effect of Ti-substitution at Mn-site for these systems. The present studies are motivated with the following possibilities:

(i) It is expected that MR of these manganites will enhance by doping of Ti^{4+} ions at Mn-site.

(ii) One can bring down Curie-temperature near to room temperature from higher temperature by doping Ti^{4+} ions at Mn-site in $La_{0.6}Ba_{0.4}MnO_3$.

(iii) One can introduce multiferroicity in these magnetic systems by doping of Ti^{4+}-ions at Mn-site, if cento-symmetry of the crystal structure is lifted.

- ✓ As we know that requirements for multiferroicity (coexistence of ferroelectricity and ferromagnetism) are contradictory. Ferroelectricity requires completely filled d-orbitals, while, magnetism requires partially empty d-orbitals. So, multiferroicity is rare in nature for single compounds.
- ✓ $BaTiO_3$ is a well known ferroelectric having tetragonal structure at room temperature with space group *P4mm* and ferroelectric to paraelectric transition at $T_C \sim 130°C$.
- ✓ Substitution of Ti-at Mn-site in Ba-doped rare earth manganites may give a way to stabilization of ferroelectric phase similar to $BaTiO_3$ in these magnetic systems as per the scheme below:

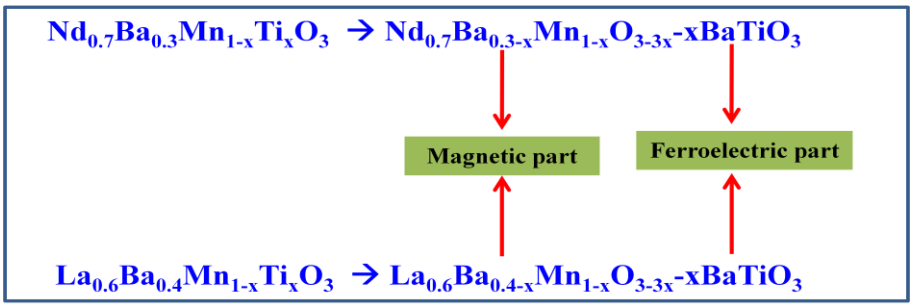

1.11. Objectives of the Present Thesis Work

Based on the detailed literature survey on bulk and nanocrystalline $R_{1-y}A_yMnO_3$ (R = La, Nd, and A = Ca, Sr, Ba) perovskite manganites, we decided to investigate following important aspects for the present Ph.D. thesis:

1. Synthesis of Ti-doped $R_{1-y}Ba_yMn_{1-x}Ti_xO_3$ (R = La, Nd) nanocrystalline and microcrystalline manganites of various particle sizes.
2. To investigate the effect of Ti-doping on crystal structure and magnetic properties of $R_{1-y}Ba_yMn_{1-x}Ti_xO_3$ (R = La, Nd) perovskite manganites.
3. To investigate the effect of crystallite size on the crystal structure and magnetic properties of these perovskite manganites.
4. To investigate the effect of temperature on the crystal structure of $Nd_{0.7}Ba_{0.3}Mn_{1-x}Ti_xO_3$ (x = 0.10) perovskite manganite.
5. To investigate the origin of suppression of spin-orbital coupling in $La_{0.6}Ba_{0.4}MnO_3$ perovskite manganite.